Supplement of Atmos. Chem. Phys., 22, 13467–13493, 2022
https://doi.org/10.5194/acp-22-13467-2022-supplement

Atmospheric Chemistry and Physics
Open Access

Supplement of

Significant formation of sulfate aerosols contributed by the heterogeneous drivers of dust surface

Tao Wang et al.

Correspondence to: Liwu Zhang (zhanglw@fudan.edu.cn)

Table of contents

Text S1. General outline

The methodology can be summarized by Fig. S1. The present study attempted to comprehensively compare the contribution of sulfate and loss of SO_2 induced by the reported gas-phase, aqueous-phase, and dust-mediated and dust-driven heterogeneous pathways. Table S1 summarizes the reported studies on the heterogeneous reaction of SO_2 on authentic particles. Table S2 summarizes the reported studies comparing heterogeneous oxidation with gas- and aqueous-phase pathways in sulfate formation.

Firstly, measurements were conducted to characterize the studied clay minerals for chemical compositions (mineral element and water-soluble ion) and physical properties (BET specific surface area, size distribution). The heterogeneous formation of sulfur-bearing species on the dust surface was *in-situ* recorded by the infrared technique. The driving factors of dust surface were identified by the correlation analysis between sulfate production rate and particle chemical composition, followed by the development of regression models to accurately predict the heterogeneous reactivity toward SO_2.

Subsequently, the infrared spectra were analyzed to obtained the particle acidity and heterogeneous kinetics. By spectrum shape, the relative abundance of S(IV) products corresponds to particle acidity. By spectrum intensity, the production rate of sulfate can be converted into reactive uptake coefficient, which can be further used to calculate the atmospheric sulfate formation rate. The association between particle acidity and sulfate formation rate supports the comparison of the available atmospheric oxidation pathways.

Finally, the typical gas-phase, aqueous-phase and dust-mediated heterogeneous pathways were assessed by the documented methodologies and parameterizations and then compared with the studied dust-driven heterogeneous pathway with respect to the lifetime of airborne SO_2 and formation rate of sulfate aerosols. Sensitivity analysis was performed to conclude how the variation of dust mass concentration influences the loss of gas-phase component and formation of particle-phase species. The joint influences of ionic strength and aerosol liquid water content on the aqueous-phase SO_2 conversion were assessed to reveal the contribution proportions of dust heterogeneous oxidation in the complex atmospheric environments. The dust-driven heterogeneous pathway was also compared with the recently discovered microdroplet interfacial SO_2 oxidations.

Text S2. Gas-phase oxidation

The following rate laws were used to quantify the sulfate production by atmospheric gas-phase oxidation.

(1) By OH (Cheng et al., 2016; Huang et al., 2019a),

$$\frac{d[SO_4^{2-}]}{dt} = k_1[OH][SO_2]$$

The effective second-order rate constant of the termolecular reaction under certain temperature can be expressed as:

$$k(T) = \left(\frac{k_0(T)[M]}{1 + \frac{k_0(T)[M]}{k_\infty(T)}} \right) F_c^{\,Z}$$

$$Z = \left\{ 1 + \left[\log_{10} \left(\frac{k_0(T)[M]}{k_\infty(T)} \right) \right]^2 \right\}^{-1}$$

Where [M] represents the concentration of N_2 and O_2, F_c (0.6) is used to calculate the dependence of k on pressure and temperature, and $k_0(T)$ and $k_\infty(T)$ are the low-pressure and high-pressure limiting rate constants, respectively. Their temperature dependence can be expressed as:

$$k_0(T) = k_0^{300} \left(\frac{T}{300} \right)^{-n}$$

$$k_\infty(T) = k_\infty^{300} \left(\frac{T}{300} \right)^{-m}$$

Where k_0^{300}=3.3 × 10^{-31} cm^6 $molecule^{-2}$ s^{-1} and n=4.3; k_∞^{300}=1.6 × 10^{-12} cm^3 $molecule^{-1}$ s^{-1} and m=0.

(2) By CIs (Mauldin III et al., 2012),

$$\frac{d[SO_4^{2-}]}{dt} = k_2[CIs][SO_2]$$

Where k_2=6.0 × 10^{-13} cm^3 $molecule^{-1}$ s^{-1}.

(3) By NO_3 (Xie, 1992),

$$\frac{d[SO_4^{2-}]}{dt} = k_3[NO_3][SO_2]$$

Where k_3=1.0 × 10^{-19} cm^3 $molecule^{-1}$ s^{-1}.

Text S3. Aqueous-phase oxidation

Text S3-1. Overview

The liquid process is largely driven by the rate of chemical reaction, as well as the mass transport in different medium and across the interface. The following equation is used to explain the mass transport effect.

$$\frac{1}{R_{H,aq}} = \frac{1}{R_{aq}} + \frac{1}{J_{aq,lim}}$$

Where $R_{H,aq}$ is the sulfate formation rate, R_{aq} is the aqueous-phase reaction rate, and $J_{aq,lim}$ is the limiting mass transfer rate. For the oxidation of S(IV) intermediates by a given oxidant O_{xi}:

$$R_{aq} = (k'[SO_2 \cdot H_2O] + k''[HSO_3^-] + k'''[SO_3^{2-}])[O_{xi}]$$

Where $[SO_2 \cdot H_2O]$, $[HSO_3^-]$, $[SO_3^{2-}]$, and $[O_{xi}]$ are the respective aqueous-phase concentrations. The k', k", and k"' are second-order reaction rate coefficients. The equilibrium of a specie X between the gas phase and aqueous phase can be expressed by the following equation.

$$X_{(g)} \leftrightarrow X_{(aq)}$$

The equilibrium is usually expressed by the so-called Henry's law coefficient H(X), and the temperature-dependent Henry's law constants are listed in Table S3.

$$[X_{(aq)}] = p(X) \cdot H(X)$$

Where $[X_{(aq)}]$ is the aqueous-phase concentration of X (mol L^{-1}), $p(X)$ is the partial pressure of X in the bulk gas phase (atm), and $H(X)$ (M atm^{-1}) is the effective Henry's law constant.

On the other hand, the limiting mass transfer rate $J_{aq,lim}$ (M s^{-1}) is calculated by:

$$J_{aq,lim} = \min\{J_{aq}(SO_2), J_{aq}(O_{xi})\}$$

$$J_{aq}(X) = k_{MT}(X) \cdot p(X) \cdot H(X)$$

Where X refers to SO_2 or oxidant O_{xi}. The mass transfer rate coefficient k_{MT} (s^{-1}) can be calculated via

$$k_{MT}(X) = \left[\frac{R_P^2}{3D_g} + \frac{4R_P}{3\alpha v}\right]^{-1}$$

Where R_p is the droplet particle radius (m), D_g is the gas-phase molecular diffusion coefficient (m^2 s^{-1}), v is the mean molecular speed of X (m s^{-1}), α is the mass accommodation coefficient of X on the aerosol droplet surface (dimensionless). Aqueous-phase mass transfer can be ignored for the size range considered here. An equivalent R_p of 0.15 μm was assumed for aerosol droplets as previously selected (Cheng et al., 2016; Liu et al., 2021). The D_g and α values are determined by the following methods, and the final calculation results are shown in Table S4.

Some D_g values were experimentally determined and can be used in this study after temperature corrections. The association between the diffusion coefficient (D) at 296 K and that under the studied temperature (T) can be expressed as:

$$D(296K) = D(T) \times \left(\frac{296}{T}\right)^{1.75}$$

Other D_g values can be estimated by Fuller's method (Fuller et al., 1969; Tang et al., 2014).

$$\frac{1}{D(X, Air, H_2O)} = \frac{1-x}{D(X, Air)} + \frac{x}{D(X, H_2O)}$$

Where D(X, Air, H_2O) represents the diffusion coefficient of gaseous oxidant X in the binary mixture of air and H_2O (Torr cm^{-2} s^{-1}) at the temperature of T (K). Moreover, x is the molar fraction of H_2O in the

humidified air and can be calculated by the saturated vapor pressure (p) of H_2O at certain temperature, as described by Antoine equation (lgp=7.07406-1657.46/(T+227.02), 10℃≤T≤168℃). The molar fraction of H_2O under the experimental temperature (296.8K) and relative humidity (50%) was calculated to be 1.443%. The D(X, Air) is given by:

$$D(X, Air)\frac{1.0868 \times T^{1.75}}{\sqrt{m(X, Air)}(\sqrt[3]{V_X} + \sqrt[3]{V_{Air}})^2}$$

$$m(X, Air) = \frac{2}{1/m_X + 1/m_{Air}}$$

Where m_X and m_{Air} are the respective molecular weights (g mol^{-1}) of X and ambient air. The same is true for D(X, H_2O). The diffusion volume of a molecule can be calculated by summing the diffusion values of the atoms it contains.

$$V = \sum n_i V_i$$

Where n_i is the number of atom with a diffusion volume of V_i included in the molecule. In the present research, the diffusion volumes of O_3, HOCl, CH_3OOH, CH_3COOOH, air and H_2O are estimated to be 18.33, 29.42, 37.36, 59.37, 19.7 and 13.1, respectively.

Mass accommodation coefficient, α, reflects the possibility of reactant molecules entering into the liquid phase and acts as another important factor for the estimation of k_{MT}. The temperature-dependent α can be described by the following equation (Worsnop et al., 1989; Jayne et al., 1991; Magi et al., 1997).

$$\ln\frac{\alpha}{1-\alpha} = -\frac{\Delta G}{RT}$$

Where ΔG is the Gibbs free energy and expressed as $\Delta G = \Delta H - T\Delta S$, T is the reaction temperature and R is gas constant.

Text S3-2. Ionization equilibrium

The dissolved SO_2 undergoes aqueous-phase ionization, and this equilibrium process can be described by the following equations. The K_{s1} and K_{s2} are 1.3×10^{-2} and 6.6×10^{-8} at 298 K, respectively.

$$K_{s1} = \frac{[H^+][HSO_3^-]}{[SO_2 \cdot H_2O]}$$

$$K_{s2} = \frac{[H^+][SO_3^{2-}]}{[HSO_3^-]}$$

Therefore, the concentrations of the diverse S(IV) species in liquid media can be calculated by the following equations.

$$[SO_2 \cdot H_2O] = H_{SO_2} p_{SO_2}$$

$$[HSO_3^-] = \frac{K_{s1}[SO_2 \cdot H_2O]}{[H^+]} = \frac{H_{SO_2} K_{s1} p_{SO_2}}{[H^+]}$$

$$[SO_3^{2-}] = \frac{K_{s2}[HSO_3^-]}{[H^+]} = \frac{H_{SO_2} K_{s1} K_{s2} p_{SO_2}}{[H^+]^2}$$

The concentration of total dissolved sulfur in solution, denoted as $[S(IV)]$, equals to

$$[S(IV)] = H_{SO_2} p_{SO_2}\left[1 + \frac{K_{s1}}{[H^+]} + \frac{K_{s1}K_{s2}}{[H^+]^2}\right]$$

Thus,

$$pH = -\lg[H^+] = -\lg(K_{s1}K_{s2}ratio)^{\frac{1}{2}}$$

Where ratio=$[SO_2 \cdot H_2O]/[SO_3^{2-}]$.

This equation can be used to calculate the acidity of the reacted dust according to the relative abundance of the formed $SO_2{\cdot}H_2O$ and SO_3^{2-}, which is assumed to be equivalent to the ratio of the integral areas of their characteristic peaks.

The Henry's law constant (H) and ionization constant (K) are both equilibrium constants in nature, and thus can be temperature-corrected based on the Van't Hoff equation.

$$H(T) = H(T_0)\exp\left[-\frac{\Delta H_{298K}}{R}\left(\frac{1}{T}-\frac{1}{T_0}\right)\right]$$

Where T_0=298 K. The same is true for K(T).

Text S3-3. Reaction rate constant

The following rate laws are used to quantify the sulfate formation by different oxidants. The rate constants discussed below correspond to the temperature of 298K, followed by the E/R values for temperature dependence if available.

(1) By ozone (O_3) (Seinfeld and Pandis, 2016):

$$\frac{d[SO_4^{2-}]}{dt} = (k_4[SO_2 \cdot H_2O] + k_5[HSO_3^-] + k_6[SO_3^{2-}])([O_{3(aq)}])$$

Where k_4=2.4 × 10^4 M^{-1} s^{-1}, k_5=3.7 × 10^5 M^{-1} s^{-1} (E/R=5530 K), k_6=1.5 × 10^9 M^{-1} s^{-1} (E/R=5280 K).

(2) By hydrogen peroxide (H_2O_2) (McArdle and Hoffmann, 1983; Seinfeld and Pandis, 2016):

$$\frac{d[SO_4^{2-}]}{dt} = \left(k_7[H^+][HSO_3^-]\left[H_2O_{2(aq)}\right]\right)/([1 + K_1[H^+])$$

Where k_7=7.45 × 10^7 M^{-1} s^{-1} (E/R=4430 K), K_1=13 M^{-1}.

(3) By O_2 catalyzed by transition metal ions (TMIs) (Ibusuki and Takeuchi, 1987):

$$\frac{d[SO_4^{2-}]}{dt} = k_8[H^+]^{-0.74}[Mn^{2+}][Fe^{3+}][S(IV)] \quad (pH \le 4.2)$$

$$\frac{d[SO_4^{2-}]}{dt} = k_9[H^+]^{0.67}[Mn^{2+}][Fe^{3+}][S(IV)] \quad (pH > 4.2)$$

Where k_8=4.17 × 10^7 M^{-1} s^{-1} (E/R=8432 K), k_9=2.81 × 10^{13} M^{-1} s^{-1} (E/R=8432 K).

(4) By nitrogen dioxide (NO_2) (Clifton et al., 1988):

The reaction rate constant of the NO_2-initiated oxidation was experimentally determined by Clifton et al. (1988). They reported that the k_{10} in the following equation increases with pH that ranges from 5.3 to 8.7. The experimental data can be linearly fitted to predict the oxidizing capacity as previously reported (Song et al., 2021).

$$\frac{d[SO_4^{2-}]}{dt} = k_{10}\left[NO_{2(aq)}\right][S(IV)]$$

Where, $k_{10}\ (M^{-1}s^{-1}) = \begin{cases} 1.24 \times 10^7 & (pH < 5.3) \\ (0.1265pH + 0.5697) \times 10^7 & (5.3 \le pH \le 8.0) \end{cases}$

(5) By hypochlorous acid (HOCl) (Liu and Abbatt, 2020):

$$\frac{d[SO_4^{2-}]}{dt} = (k_{11}[HSO_3^-] + k_{12}[SO_3^{2-}])\left(\left[HOCl_{(aq)}\right]\right)$$

Where k_{11}=2.8 × 10^5 M^{-1} s^{-1}, k_{12}=7.6 × 10^8 M^{-1} s^{-1}.

(6) By hypobromous acid (HOBr) (Liu and Abbatt, 2020):

$$\frac{d[SO_4^{2-}]}{dt} = (k_{13}[HSO_3^-] + k_{14}[SO_3^{2-}])([HOBr_{(aq)}])$$

Where k_{13}=2.6 × 10^7 M^{-1} s^{-1}, k_{14}=5.0 × 10^9 M^{-1} s^{-1}。

(7) By hydroperoxide (CH_3OOH) (Walcek and Taylor, 1986; Lind et al., 1987):

$$\frac{d[SO_4^{2-}]}{dt} = k_{15}[H^+][HSO_3^-][CH_3OOH_{(aq)}]$$

Where k_{15}=1.85 × 10^7 M^{-1} s^{-1} (E/R=3801 K).

(8) By peroxyacetic acid (CH_3COOOH) (Walcek and Taylor, 1986; Lind et al., 1987):

$$\frac{d[SO_4^{2-}]}{dt} = (K_2 + k_{16}[H^+])[HSO_3^-][CH_3COOOH_{(aq)}]$$

Where k_{16}=4.83 × 10^7 M^{-1} s^{-1} (E/R=3993 K), K_2=601 M^{-1} s^{-1}.

(9) By nitrous acid (HONO) (RobbinMartin et al., 1981; Oblath et al., 1982):

$$\frac{d[SO_4^{2-}]}{dt} = k_{17}[H^+]^{0.5}[S(IV)][HONO]_{aq} \qquad (pH < 3.2)$$

$$\frac{d[SO_4^{2-}]}{dt} = k_{18}[H^+][S(IV)][HONO]_{aq} \qquad (pH \geq 3.2)$$

Where k_{17}=142 $M^{-1.5}$ s^{-1}, k_{18}=3800 M^{-2} s^{-1}.

(10) By peroxynitric acid (HO_2NO_2) (Warneck, 1999; Berglen et al., 2004; Tilgner et al., 2021):

$$\frac{d[SO_4^{2-}]}{dt} = k_{19}[HSO_3^-]\left[HO_2NO_{2(aq)}\right]$$

Where k_{19}=3.1 × 10^5 M^{-1} s^{-1}.

(11) By excited triplet states of photosensitizers (T*) (Wang et al., 2020):

$$\frac{d[SO_4^{2-}]}{dt} = k_{20}([SO_2 \cdot H_2O] + [HSO_3^-])[T^*]$$

Where k_{20}=1.3 × 10^8 M^{-1} s^{-1}.

(12) By nitrate photolysis:

The pH-dependent sulfate formation derived by the photolysis of nitrate can be assessed by the kinetic model reported by Masao et al. (2019a; 2019b) and Zheng et al. (2020).

According to the Arrhenius equation, the dependence of the kinetic constant k on temperature T can be expressed by the equation as follows:

$$k(T) = k(T_0)\exp\left[-\frac{E}{R}\left(\frac{1}{T} - \frac{1}{T_0}\right)\right] \qquad (T_0 = 298\ K)$$

Here, we changed the unit of sulfate formation rate from M s^{-1} in liquid water to μg m^{-3} h^{-1} in ambient air by:

$$\frac{d[SO_4^{2-}]}{dt}(\mu g\ m^{-3}\ h^{-1}) = \frac{d[SO_4^{2-}]}{dt}(M\ s^{-1}) \times 96 g\ mol^{-1} \times \frac{ALWC}{\rho_{H_2O}}$$

Where ALWC is the aerosol liquid water content (μg m^{-3}), and ρ_{H_2O} is water density (g cm^{-3}).

Text S3-4. Effect of ionic strength

Ionic strength (I) is closely associated with the aqueous-phase sulfate formation as it influences both of Henry's law coefficient and reaction rate constant. Herein, the aqueous SO_2 oxidation by H_2O_2, NO_2, O_3, and TMI-catalyzed O_2 are taken into account for their ionic strength dependence on sulfate formation. In

this work, the aqueous-phase parameters were adjusted by temperature at first, followed by the ionic strength correlations.

(1) **SO_2**

The ionic strength dependences of SO_2 were described by Millero et al. (1989):

$$\lg\left(\frac{H_{SO_2}}{H_{SO_2}^{I=0}}\right) = \left(\frac{22.3}{T} - 0.0997\right) I$$

$$\lg\left(\frac{K_{a1}^{*}}{K_{a1}^{I=0}}\right) = 0.5\sqrt{I} - 0.31I$$

$$\lg\left(\frac{K_{a2}^{*}}{K_{a2}^{I=0}}\right) = 1.052\sqrt{I} - 0.36I$$

(2) **H_2O_2**

The effect of ionic strength on the gas-liquid equilibrium of H_2O_2 was investigated by Ali et al. (2014) and concluded by Liu et al. (2020).

$$\frac{H_{H_2O_2}}{H_{H_2O_2}^{I=0}} = 1 - 1.414 \times 10^{-3} I^2 + 0.121I$$

The effect of ionic strength on the reaction rate constant related to H_2O_2 was experimentally proved by Maaβ et al. (1999):

$$\lg\left(\frac{k}{k^{I=0}}\right) = 0.36I - \frac{1.018\sqrt{I}}{1 + 0.17\sqrt{I}}$$

In addition, Liu et al. (2020) found that the ionic strength effects on the oxidation of SO_2 in the droplets that buffered by malonic acid may not be accurately predicted by the model developed for bulk solutions. Song et al. (2021) fitted those results by:

$$\ln\left(\frac{k}{k^{I=0}}\right) = 30.374 - \frac{6824.2068}{215.365 + I}$$

(3) **NO_2**

The effect of ionic strength on the Henry's law coefficient of NO_2 was not available due to the lack of laboratory data. Moreover, the dependence on reaction rate constant was theoretically determined by Cheng at al. (2016) to be 0.5 M^{-1} and assumed by Song et al. (2021) to be 0.01 M^{-1}. The latter value is used by this work.

$$\lg\left(\frac{k}{k^{I=0}}\right) = b_1 I \ (b_1 > 0)$$

(4) **O_3**

Kosak-Channing and Helz (1983) investigated the equilibrium between gaseous and dissolved O_3 under different ionic strength and temperature conditions, and obtained the multivariable linear regression:

$$H_{O_3} = \left[\exp\left(-\frac{2297}{T} + 2.659I - 688\frac{I}{T} + 12.19\right)\right]^{-1}$$

The effect of ionic strength on the oxidation of SO_2 by O_3 was investigated by Maahs (1983) and Lagrange at al. (1994), as shown by the following equations. A medium value of b_2=1.0 and b_3=1.94 are recommended for the complex aerosol media to show the general pattern (Song et al., 2021). In this work, we used the Davies equation to display the ion strength dependence of the oxidation by O_3.

$$\lg\left(\frac{k}{k^{I=0}}\right) = b_2\left(\frac{\sqrt{I}}{1 + \sqrt{I}} - 0.3I\right) \ (0.7 \le b_2 \le 1.3)$$

$$\frac{k}{k^{I=0}} = 1 + b_3 I \ (1.34 \le b_3 \le 6.13)$$

(5) **O_2 catalyzed by TMIs**

Martin and Hill (1967; 1987) built the relationship between I and k for the oxidation of SO_2 by the TMI-catalyzed O_2, as shown follows. The b_4 was experimentally determined to be -3.02 (Liu et al., 2020), within the range of -2 for Fe^{3+} and -4 for Mn^{2+}.

$$\lg\left(\frac{k}{k^{I=0}}\right) = b_4 \frac{\sqrt{I}}{1+\sqrt{I}} \quad (-4 \le b_4 \le -2)$$

Text S4. Oxidant concentration determination

Text S4-1. Gas-phase oxidants

The concentration data were derived from the atmospheric observation campaigns performed in Beijing, North China. Specifically, the measurements for warm seasons were considered in priority to correspond the experimental temperature of this study. Additionally, considering the relatively high irradiance used in the laboratory experiments, the oxidant concentrations involved in the assessments of the diurnal gas- and aqueous-phase pathways were selected from the observations performed at noon time. The relevant data are presented in Table S5.

The presence of dust particles would cause the loss of gaseous reactive species, and therefore the oxidant concentration can be expressed by:

$$[\mathrm{Oxi}] = [\mathrm{Oxi}]_0 - [\mathrm{Oxi}]_a$$

Where [Oxi] is the atmospheric mass concentration of the specific gas-phase oxidant, and the subscripts "0" and "a" indicate the oxidant concentration in the absence of dust (listed in Table S5) and the concentration of the surface assumed oxidants calculated by:

$$\frac{d[\mathrm{Oxi}]_a}{dt} = k[\mathrm{Oxi}]$$

Where k is the pseudo-first-order rate coefficient (s^{-1}) parametrizing the heterogeneous uptake of gases onto the dust surface.

Thus,

$$[\mathrm{Oxi}]_a = \int_0^t k[\mathrm{Oxi}]\,dt$$

The calculation formulation of k(s^{-1}) is given by:

$$k = \left(\frac{r_p}{D_g} + \frac{4}{v\gamma}\right)^{-1} S_p$$

Where k is the loss rate of the species from the gas phase (s^{-1}), r_p is the effective particle radius (m), D_g is the gas-phase diffusion coefficient of the studied trace gas ($m^2\ h^{-1}$), v is the molecular velocity (m s^{-1}), γ is the reactive uptake coefficient (dimensionless), S_p is the particle surface area density ($m^2\ m^{-3}$). According to the previous publications (Bian and Zender, 2003; Crowley et al., 2010; Wang et al., 2012; Kumar et al., 2014; Tang et al., 2017; Li et al., 2017a), the γ values for the heterogenous uptake of OH, NO_3, H_2O_2, O_3, NO_2, HONO, HOCl, HOBr, CH_3OOH, and CH_3COOOH are set to be 1.0×10^{-3}, 3.0×10^{-3}, 1.0×10^{-4}, 5.0×10^{-5}, 4.4×10^{-5}, 1.0×10^{-6}, 9.1×10^{-6}, 9.1×10^{-6}, 1.0×10^{-4}, and 2.4×10^{-4}, respectively.

Besides the adsorption of gas-phase oxidants over the dust surfaces, there is desorption of gas-phase OH from the irradiated mineral dust, followed by the formation of H_2SO_4 that induces new particle formation event (Dupart et al., 2012; Chen et al., 2021). Herein, the number concentration of the newly formed

particles attributed to the irradiated dust particle surface was parameterized by the published laboratory data, and its correlation with the H_2SO_4 concentration was reported by Sipilä et al. (2010). In this study, we assumed that one OH was consumed per H_2SO_4 molecule produced.

Text S4-2. Nitrate photolysis

Based on the laboratory experiments by Gen et al. (2019a), Zheng et al. (2020) derived a quantitative methodology to calculate the sulfate formation rate attributed to the photolysis of nitrate by assuming that the sulfate formation can be initiated by the produced N(III) species including NO_2^- and HONO:

$$\frac{d[SO_4^{2-}]}{dt} = \gamma_{SO_2} \times v \times \frac{S_p}{4} \times [SO_2]$$

$$\gamma_{SO_2} = 1.64 \times P_{NO_3^-} \times \frac{K_{HNO_2}}{K_{HNO_2} + [H^+]}$$

$$P_{NO_3^-} = [NO_3^-] \times J_{HNO_3} \times EF$$

$$K_{HNO_2} = 5.9 \times 10^{-4} \times \exp\left[-1760\left(\frac{1}{T} - \frac{1}{T_0}\right)\right]$$

Where γ_{SO_2} is the reactive uptake coefficient of SO_2 (dimensionless), v is the molecular velocity of SO_2 (m s^{-1}), S_p is the particle surface area density (m^2 m^{-3}), $[SO_2]$ is the atmospheric SO_2 concentration (μg m^{-3}), $P_{NO_3^-}$ is the NO_3^- photolysis rate (M s^{-1}), $[NO_3^-]$ is the concentration of NO_3^- (M), J_{HNO_3} is the photolysis rate of HNO_3 (s^{-1}), EF is the enhancement factor of $J_{NO_3^-}$ comparing the process on particle surface with that in the gaseous medium (dimensionless), K_{HNO_2} is the temperature-dependent dissociation equilibrium constant of HNO_2 (Nair and Peters, 1989), $[H^+]$ is the molar concentration of hydrogen ion in the aerosol water (M). The photolysis rate was determined under tropical noontime conditions where the rate constant is ~ 3×10^{-7} s^{-1} for aqueous nitrate and ~ 7×10^{-7} s^{-1} for gaseous HNO_3 (Jankowski et al., 2000; Ye et al., 2016). The concentration of aqueous nitrate can be calculated by the selected NO_2 concentration and the reported NOR values (~ 0.2) in Beijing, China (Li et al., 2013; Zhang et al., 2018). Based on the recent laboratory works on atmospherically relevant droplets (Shi et al., 2021), the nitrate photolysis rate enhancement factor is generally lower than 2.0 under the wide range of experimental RH, and this upper limit value is used in the present study.

Text S4-3. Transition metal ions

The concentrations of Mn^{2+} and Fe^{3+} are pH-dependent and derived from the following equations.

$$[Mn^{2+}] = \min\left\{\frac{K_{sp,Mn(OH)_2}}{[OH^-]^2}, L_{Mn^{2+}}\right\}$$

$$[Fe^{3+}] = \min\left\{\frac{K_{sp,Fe(OH)_3}}{[OH^-]^3}, L_{Fe^{3+}}\right\}$$

Where $K_{sp,Mn(OH)_2}$ and $K_{sp,Fe(OH)_3}$, the precipitation constants of $Mn(OH)_2$ and $Fe(OH)_3$, are determined to be 1.6×10^{-13} and 6.0×10^{-38}, respectively. When all $Mn(OH)_2$ and $Fe(OH)_3$ are dissolved, further decrease of pH will not increase the concentrations of Mn^{2+} and Fe^{3+}. The upper concentration limits ($L_{Mn^{2+}}$ and $L_{Fe^{3+}}$) can be calculated by the ALWC and concentrations of soluble Mn and Fe.

The concentrations of soluble Fe and Mn are dependent by the mass concentration of dust. The airborne concentration of Fe is 3.5% of total dust mass (Alexander et al., 2009; Shao et al., 2019). The atmospheric loading of elemental Mn was derived by an empirical equation bridging the common atmospheric concentrations of Fe and Mn in North China (Zhao et al., 2013), as shown follows:

$$L_{Mn^{2+}} = 0.0641 L_{Fe^{3+}} - 17.976 \quad (R^2 = 0.8492)$$

The water solubility of an aerosol metal (the ratio of water-soluble metal mass to total metal mass) was determined to be 1.2% for Fe and 40.2% for Mn, as reported by the aerosol observations in Beijing, China (Wang et al., 2015a). In the presence of 55 μg m^{-3} airborne dust, the concentrations of Fe^{3+} and Mn^{2+} are calculated to be 23.1 and 42.4 ng m^{-3}, respectively.

Text S5. Microdroplet interfacial oxidation of SO_2

Up to now, three SO_2 oxidation cases relevant to the microdroplet interface have been quantitatively investigated to highlight the interfacial roles of O_2 (Hung and Hoffmann, 2015; Hung et al., 2018), NO_2 (Liu and Abbatt, 2021; Yu, 2021) and Mn^{2+} (Wang et al., 2021) at the droplet interface. The following content was arranged to list the necessary calculation steps of the interfacial oxidation processes.

(1) O_2 at acidic interface

$$\frac{d[SO_4^{2-}]}{dt} = \frac{1/4\, vnq(4\pi {R_P}^2)}{N_A \times V_d}$$

$$q = \frac{5.6 \times 10^{-5}[H^+]^{3.7}}{[H^+]^{3.7} + 10^{-13.5}}$$

Where v is the mean molecular speed of SO_2 (m s^{-1}), n is the number concentration of molecular SO_2 (molecules m^{-3}), R_p is the droplet radius (m), N_A is Avogadro's constant (6.022×10^{23}), V_d is the volume of droplet (L $droplet^{-1}$), q is a pH-dependent efficiency factor, and $[H^+]$ is the concentration of hydrogen ion (M s^{-1}).

Very recently, Chen et al. (2022) reported a new methodology for quantifying the interfacial kinetics of O_2 emphasizing the dependence of ionic strength. The reactive uptake coefficient of the reactant gas SO_2 (γ_{SO_2}) is defined as:

$$\gamma_{SO_2} = \frac{d[SO_4^{2-}]/dt}{Z}$$

$$Z = \frac{1}{4} \times S_p \times [SO_2] \times v_{SO_2}$$

Where $d[SO_4^{2-}]/dt$ is the formation rate of interfacial sulfate (ion s^{-1} m^{-3}), S_p is the particle surface area density (m^2 m^{-3}), $[SO_2]$ is the experimental concentration of SO_2 (molecules m^{-3}), v_{SO_2} is the molecular velocity of SO_2 (m s^{-1}).

The γ_{SO_2} under a certain ionic strength I can be conversed by that at the I=0 condition.

$$\log\frac{\gamma}{\gamma_{I=0}} = mI$$

Where the $\gamma_{I=0}$ was experimentally determined as 1.626×10^{-8}, m=0.041 kg mol^{-1}.

(2) Interfacial NO_2

The aqueous-phase oxidation of SO_2 by NO_2 in bulk environment was investigated by a series of studies. Recently, Liu et al. (2021) discovered and quantified the oxidation of SO_2 by the presence of interfacial NO_2:

$$\frac{d[SO_4^{2-}]}{dt} = (k_{21}[HSO_3^-] + k_{22}[SO_3^{2-}])[NO_{2(aq)}]$$

Where k_{21}=3.0 × 10^6, k_{22}=1.4 × 10^{10} M s^{-1}.

(3) Interfacial Mn^{2+}

The interfacial oxidation of SO_2 accelerated by Mn^{2+} was recently reported by Wang et al. (2021) and further evaluated by Wang et al. (2022):

$$\frac{d[SO_4^{2-}]}{dt} = k_{23} \times f(H^+) \times f(T) \times f(I) \times [Mn^{2+}] \times [SO_2] \times S_p$$

$$f(H^+) = -\frac{1}{1 + a[H^+] + b[H^+]^2}$$

$$f(T) = e^{-\frac{E}{R}\left(\frac{1}{T} - \frac{1}{T_0}\right)}$$

Where k_{23} is the reaction rate constant (11079.30 μg m^{-3} min^{-1}), $f(H^+)$ is the function of H^+, f(T) is the function of temperature, f(I) is the enhancement factor of ionic strength and should be determined to be 1.0 under the studied experimental temperature T (K), $[Mn^{2+}]$ is the concentration of Mn^{2+} in aerosol liquid water (M), $[SO_2]$ is the mixing ratio of gaseous SO_2 (ppb), S_p is the density of particle surface area (nm^2 cm^{-3}) and is determined to be 10 cm^2 m^{-3} by referring to the simulated atmospheric conditions of North China Plain, followed by the relevant parameters of a (-8.83×10^{17}), b (-7.84×10^{21}), and E/R (11576.08 K).

(4) Interfacial Mn^{2+}

The interfacial SO_2 oxidation by Mn^{2+} was additionally described by Zhang et al. (2021) by:

$$\frac{d[SO_4^{2-}]}{dt} = 2.0 \times 10^4 \times [Mn^{2+}] \times [S(IV)]^{1.3}$$

Where $[Mn^{2+}]$ and [S(IV)] are the aqueous-phase concentrations of the corresponding species (M).

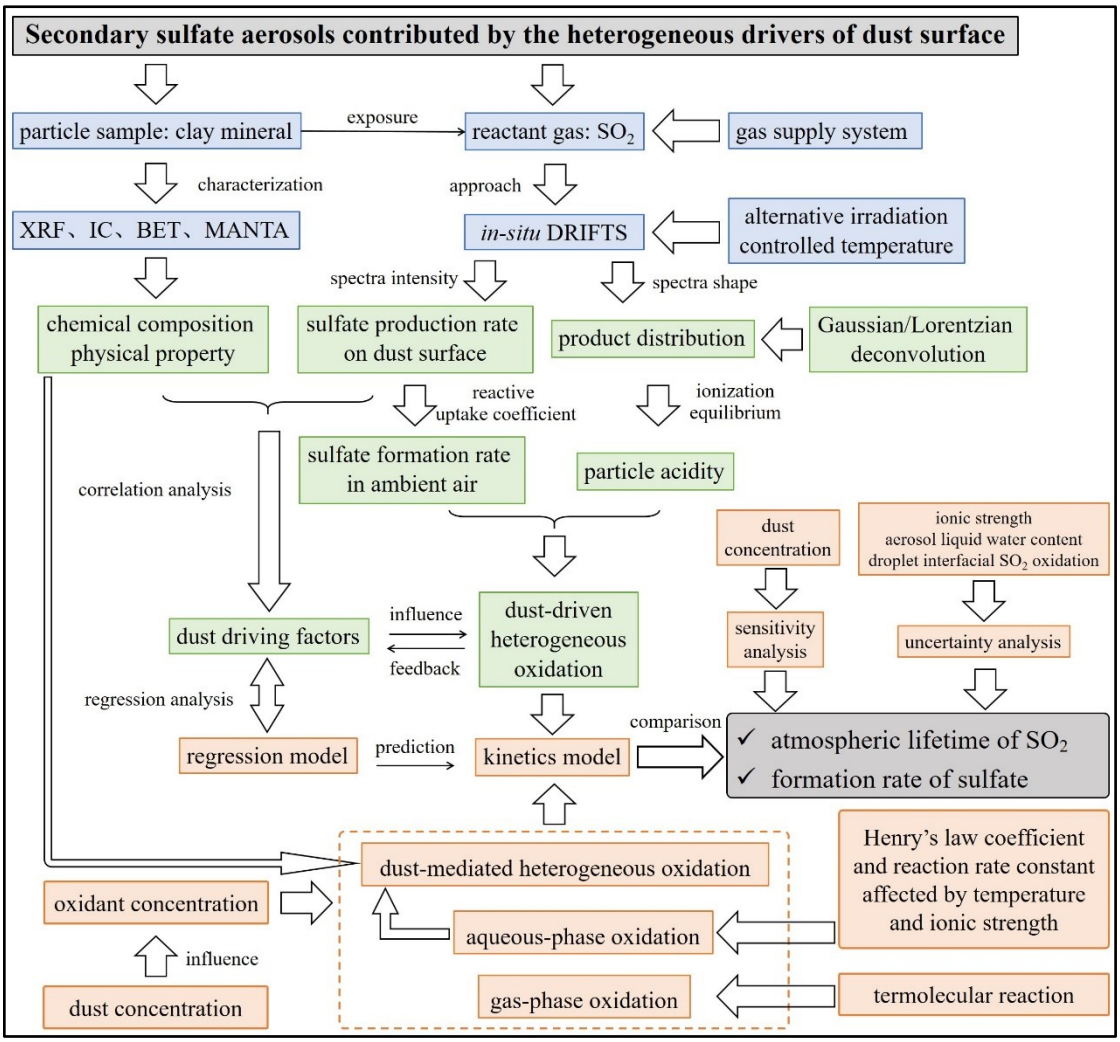

Figure S1. Schematic diagram illustrating the research topic (grey), experimental steps (blue), data analysis procedures (green), and modeling research (red).

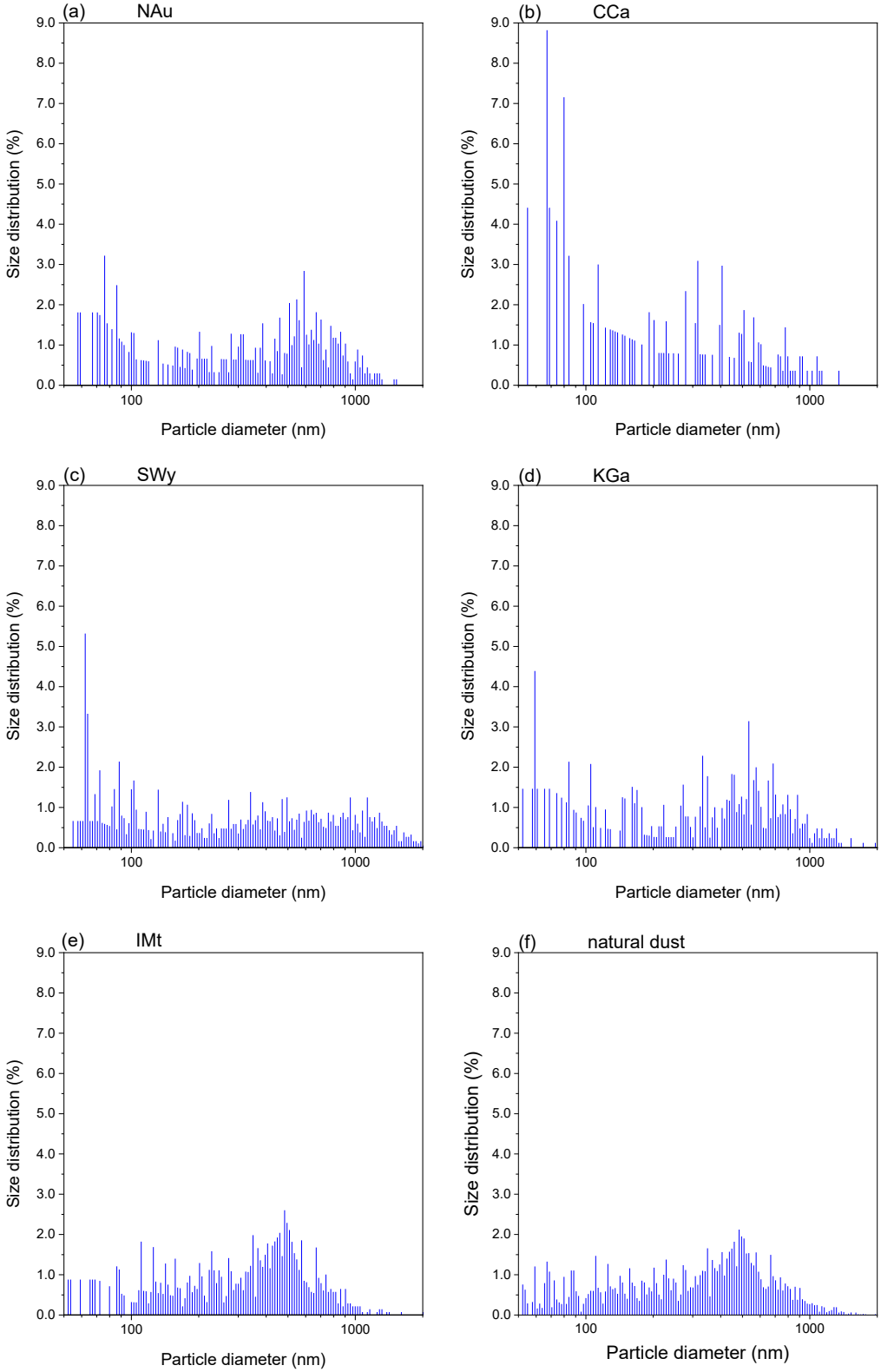

Figure S2. Size distributions of the studied particle samples.

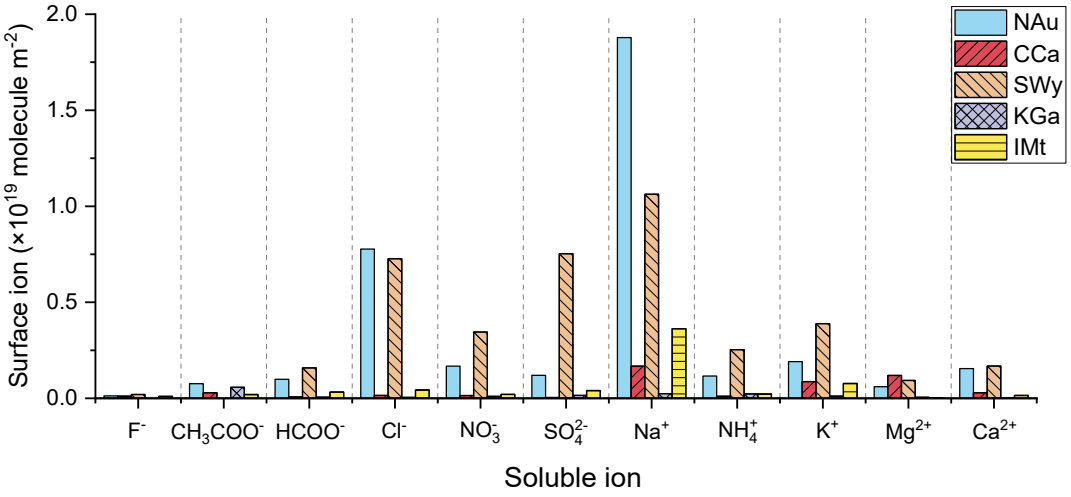

Figure S3. Water-soluble ion concentrations of the clay mineral samples.

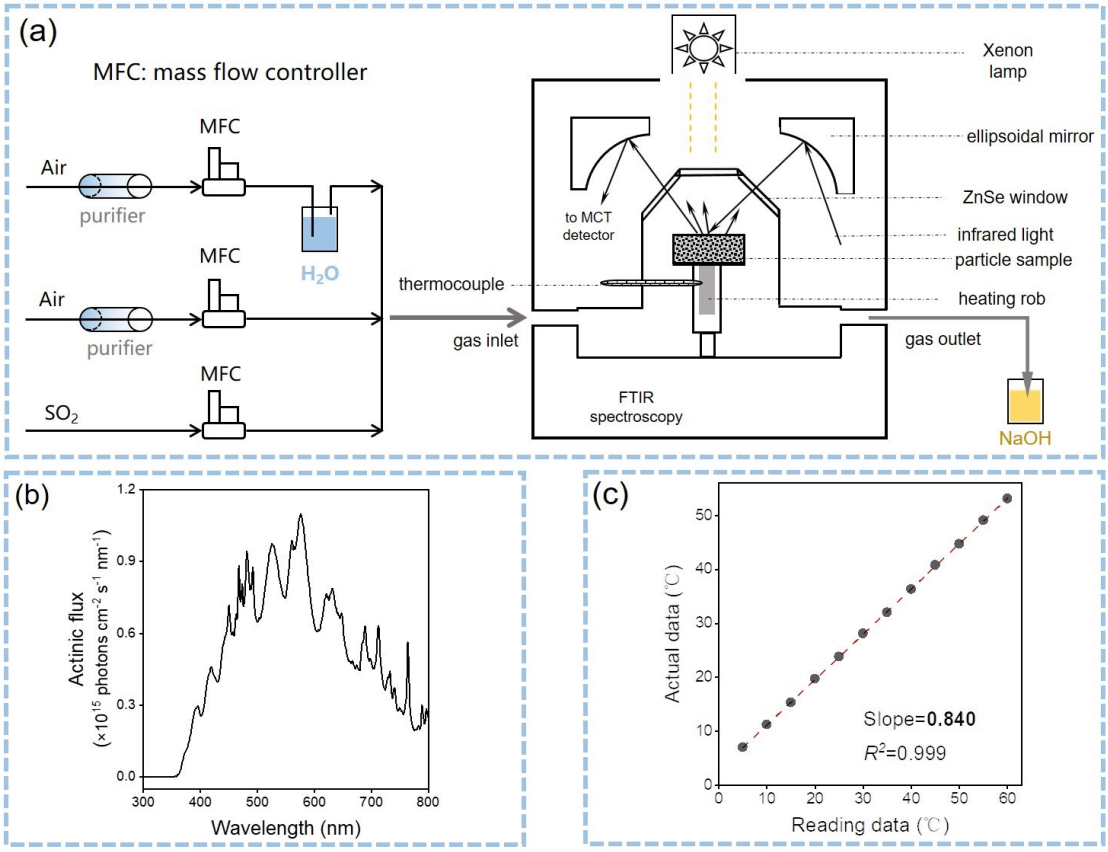

Figure S4. Experimental equipment for the heterogeneous reaction of SO_2 on dust particles. (a) Schematic diagram of the experimental setup. (b) Spectral irradiance of the Xenon lamp light. (c) Linear correlation between the reading and actual temperatures of the DRIFTS reaction chamber.

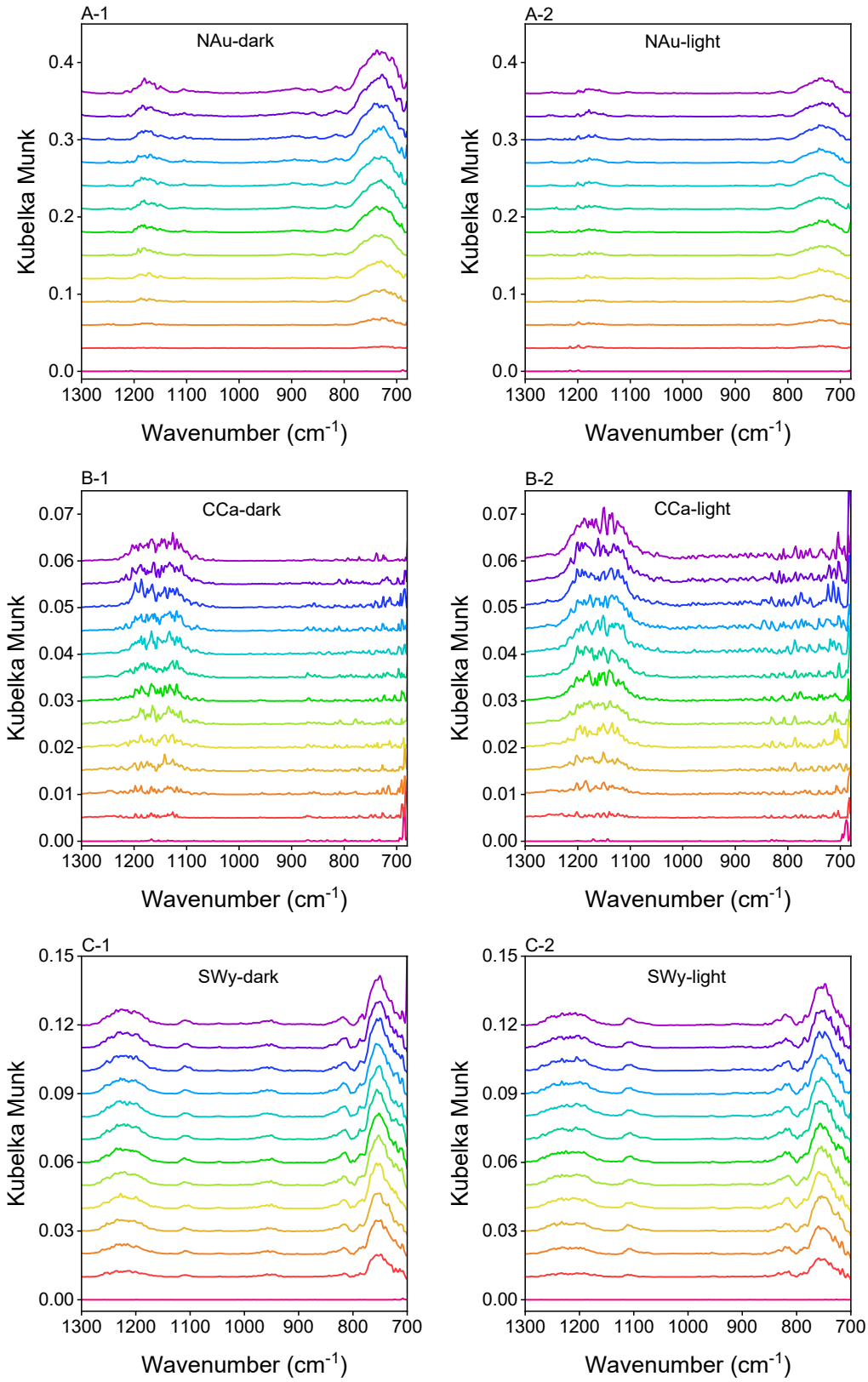

Figure S5. DRIFTS spectra recorded for the heterogeneous reaction of SO_2 on diverse clay minerals under dark and light conditions.

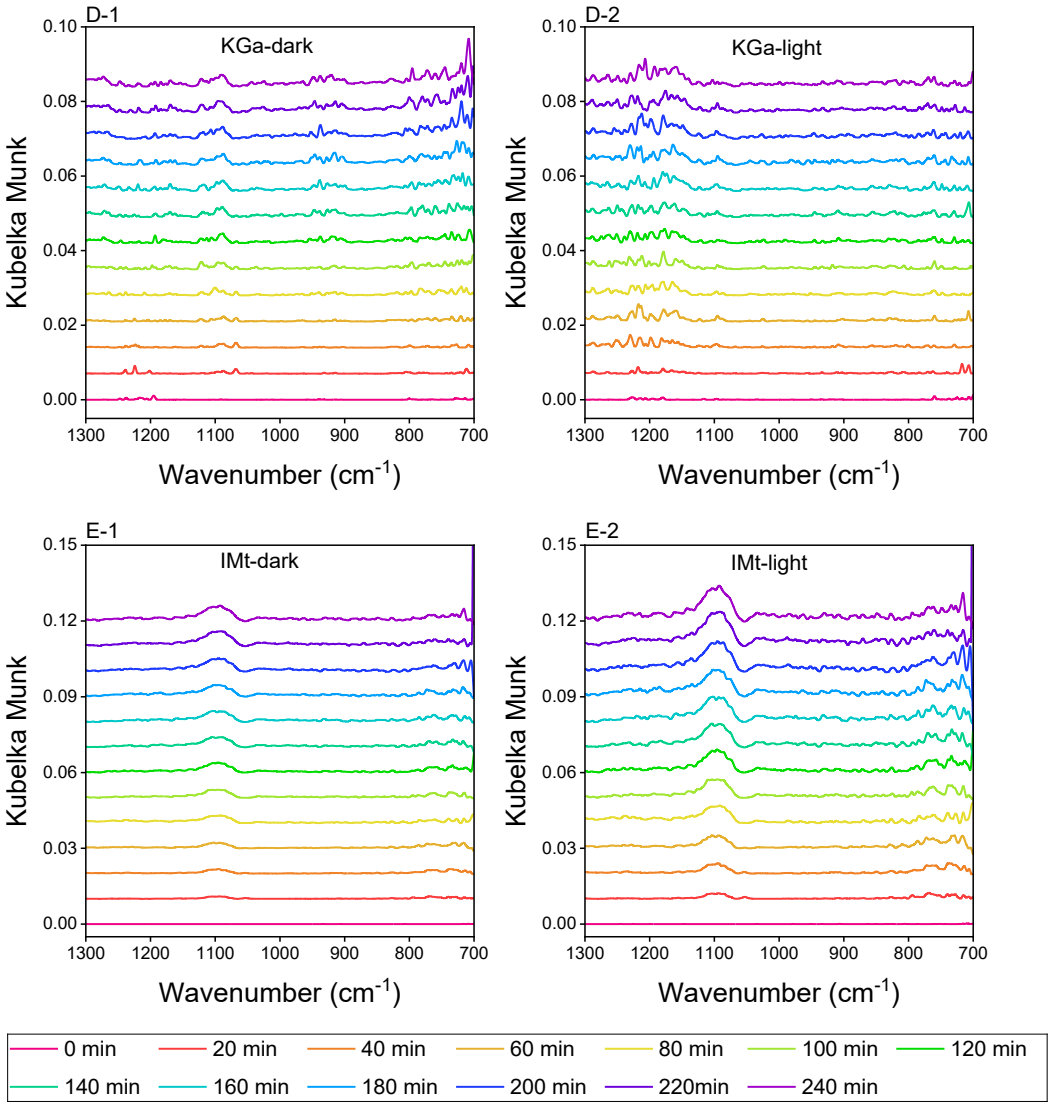

Figure S5-Continued.

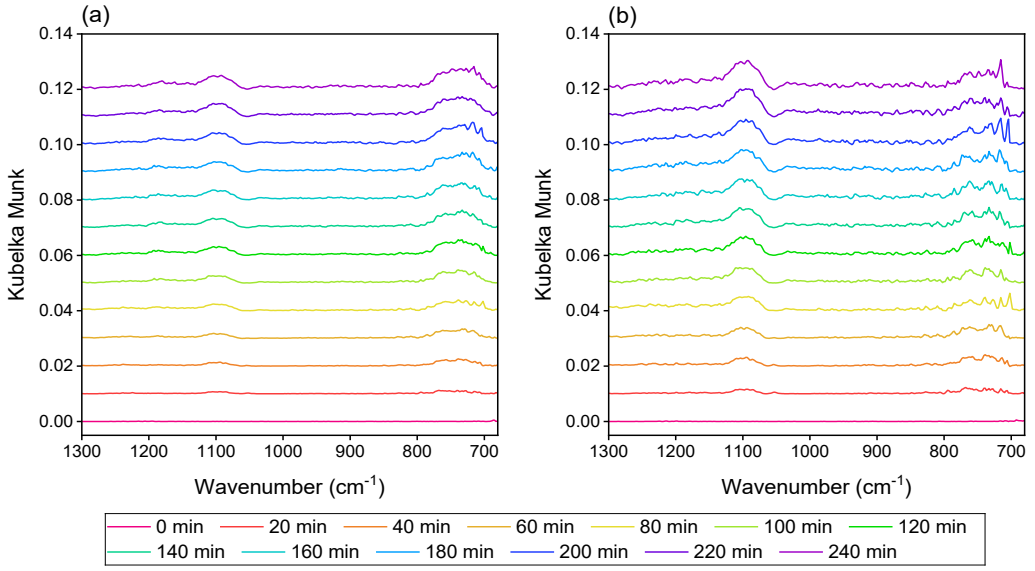

Figure S6. DRIFTS spectra recorded for the heterogeneous reaction of SO_2 on natural dust in the (a) absence and (b) presence of the simulated solar irradiation.

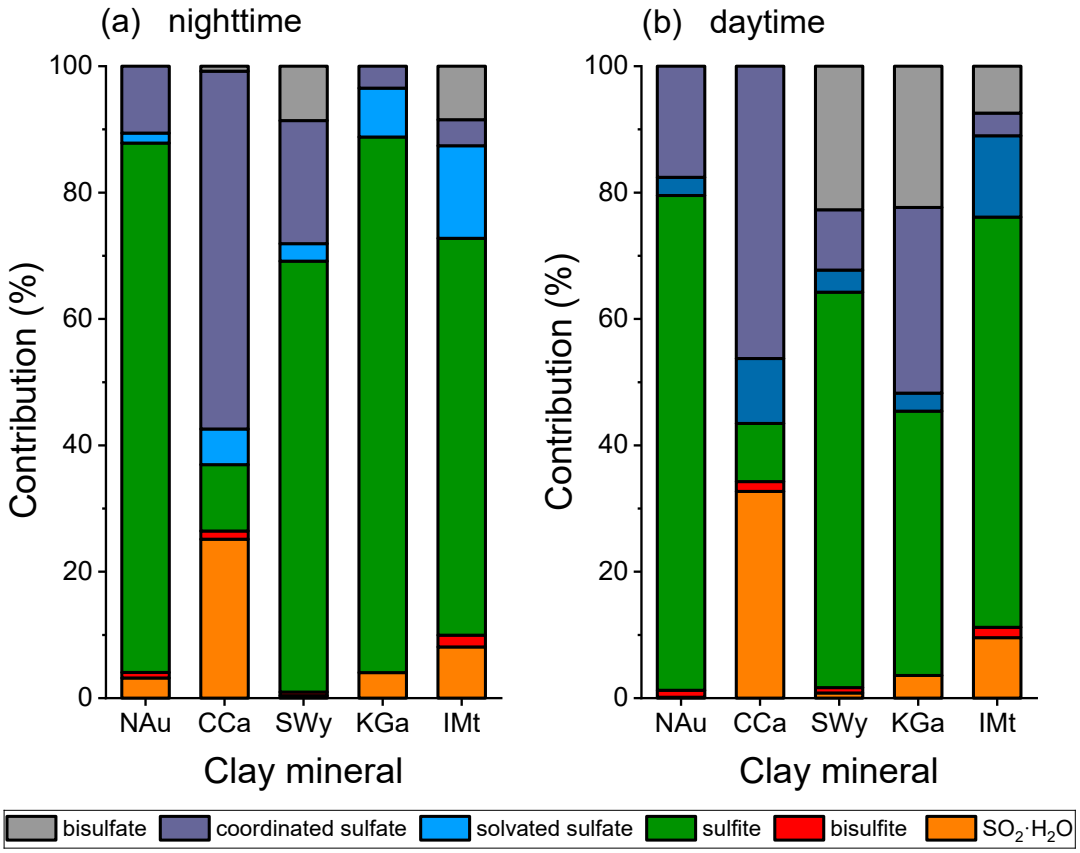

Figure S7. Relative abundance of the sulfur-containing species formed on clay minerals upon the 240 min exposure to SO_2.

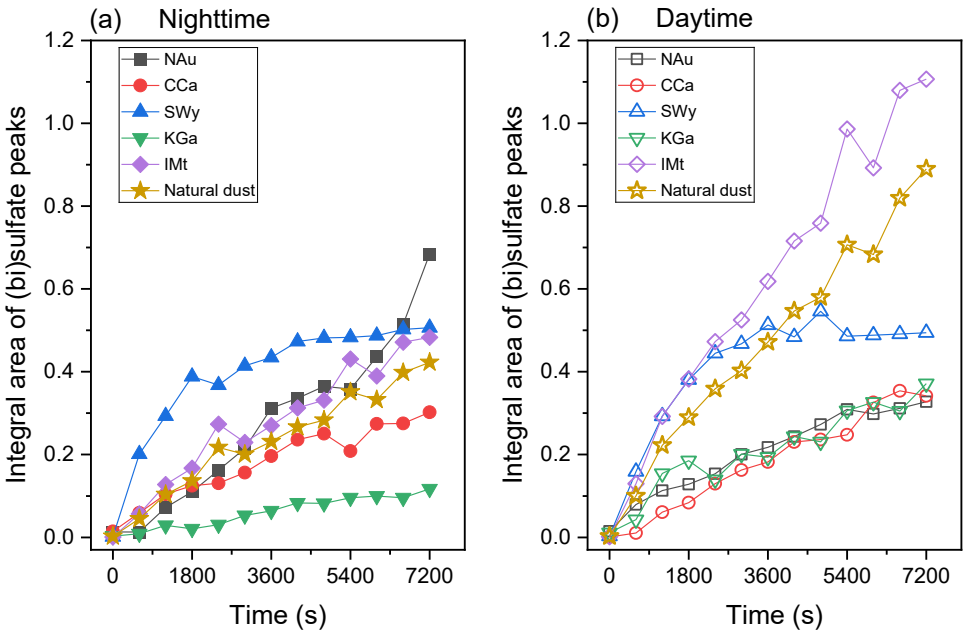

Figure S8. Integral peak area of the (bi)sulfate species formed on the clay mineral and natural dust samples as a function of reaction time.

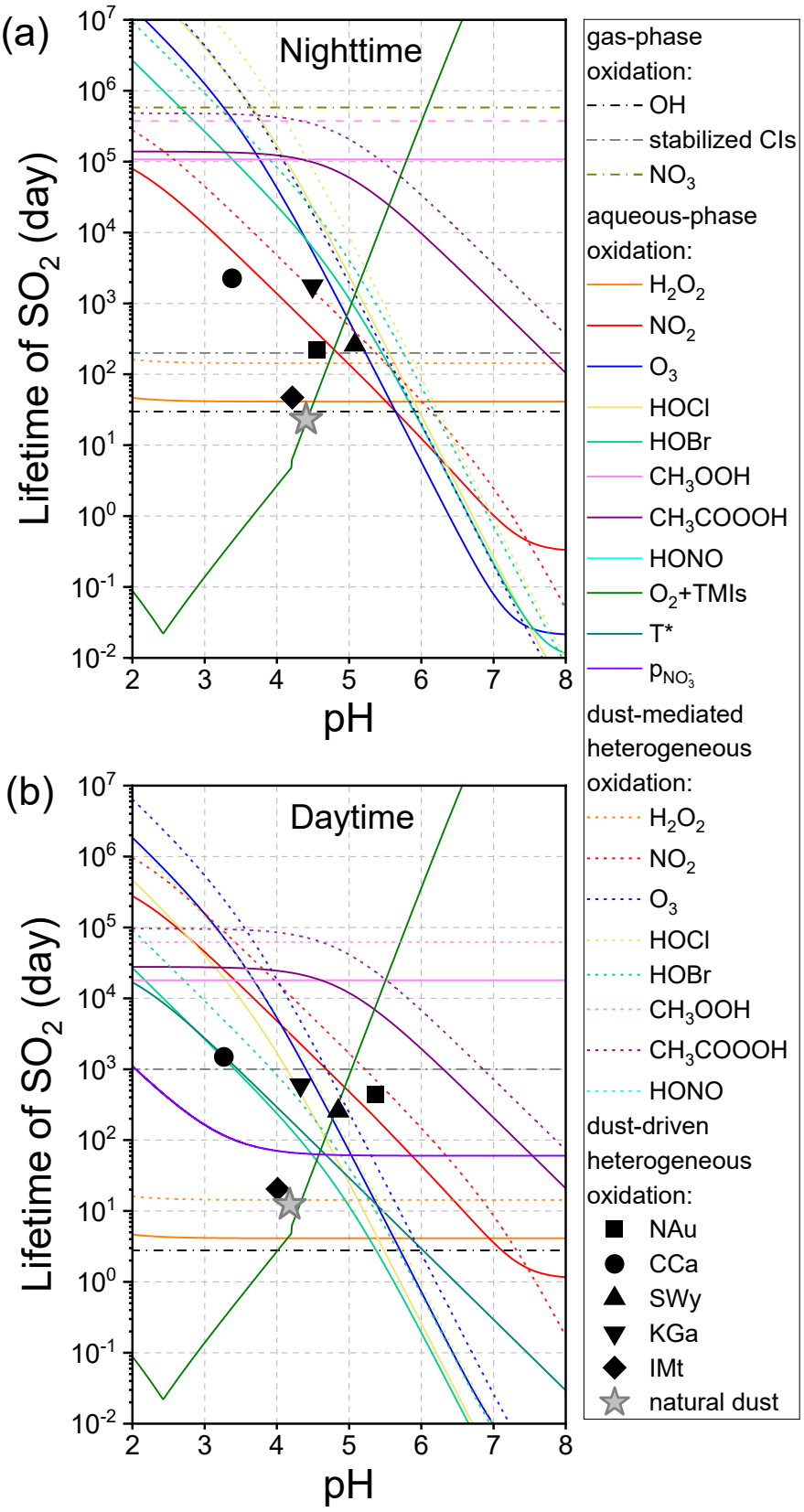

Figure S9. Particle acidity-dependent atmospheric lifetime of SO_2 induced by the typical gas-phase/ aqueous-phase/heterogeneous oxidation pathways.

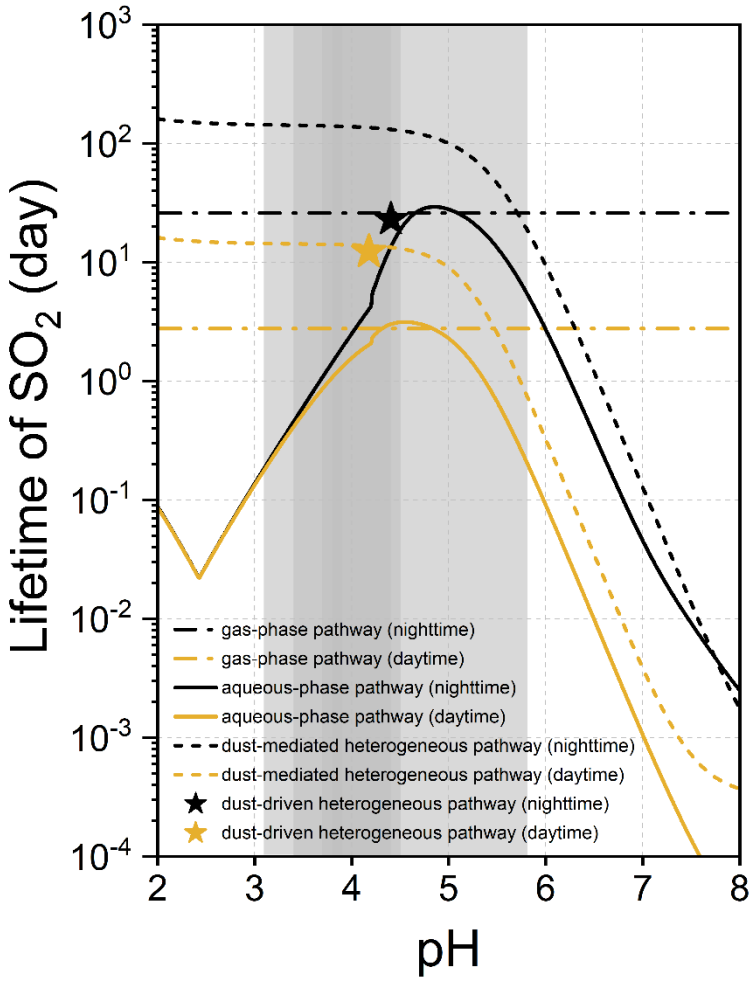

Figure S10. Lifetimes of SO_2 induced by the gas-phase, aqueous-phase, and dust-mediated and dust-driven heterogeneous chemical processes as a function of particle acidity (pH).

Gray areas indicate the pH ranges of the polluted particulate matters, with darker ones being more common (Ding et al., 2019).

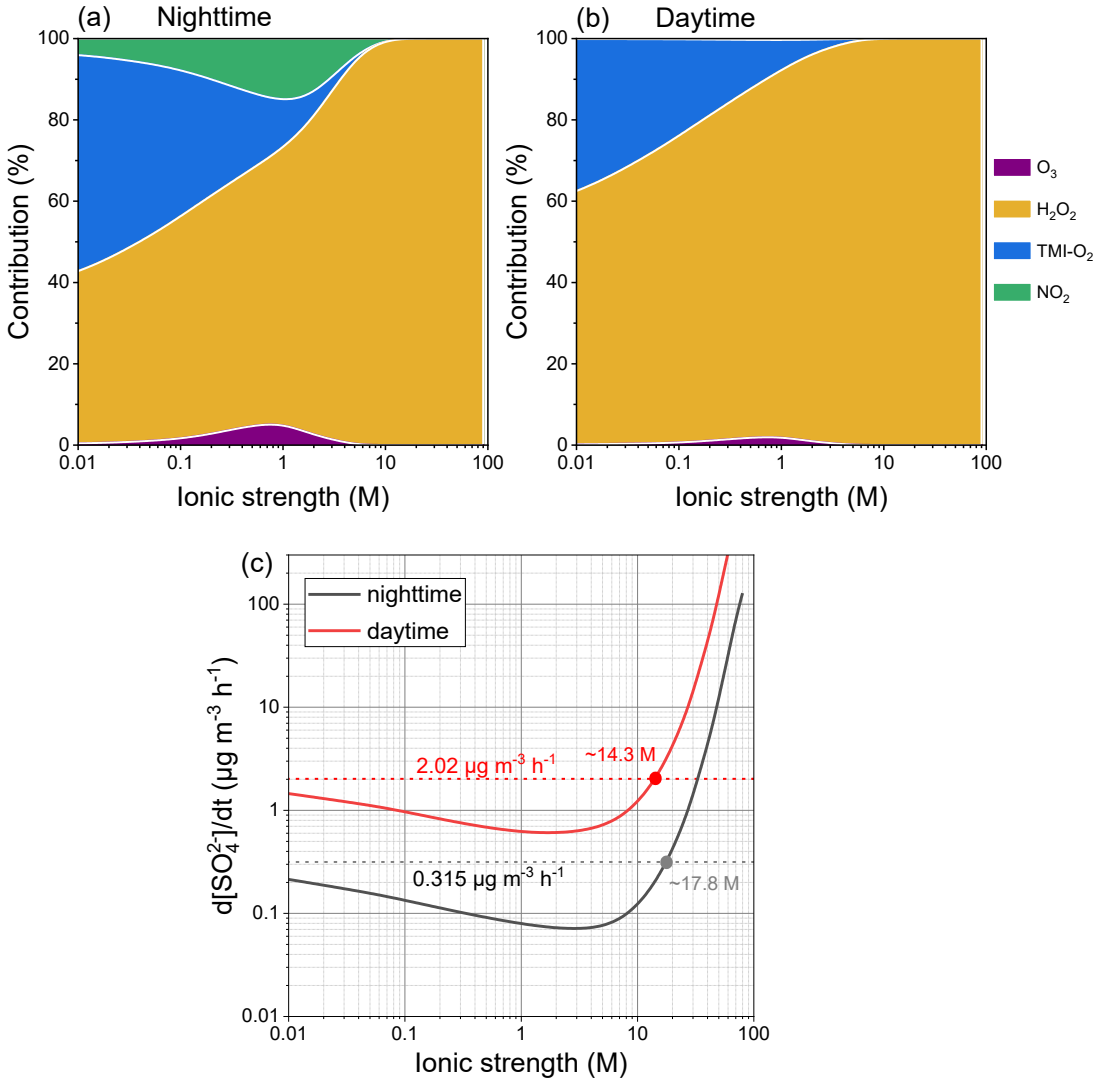

Figure S11. Effects of ionic strength on the aqueous-phase formation of sulfate.

Contribution distributions of the studied aqueous-phase pathways during (a) nighttime (pH=4.405) and (b) daytime (pH=4.177) as a function of ionic strength. (c) Aqueous-phase sulfate formation rate as a function of ionic strength (solid line) accompanied with the dash lines indicating the formation potentials calculated by the ionic strength-free settings. The intersection plots reflect the thresholds distinguishing the negative or positive effects of ionic strength. Parameter settings: ALWC=300 μg m^{-3}, concentration of SO_2: 40 ppb.

Table S1. Summary of the modeling studies comparing heterogeneous oxidation pathway with gas- and/or aqueous-phase pathways in sulfate formation.

Model description	Summary of key results	Reference
Comprehensive Air Quality Model with Extensions (CAMx)	Adding the SO_2+NO_2 reactions and increasing NH_3 emissions led to the significant model improvement. The studied heterogeneous process could account for 10.5%, 15.9%, and 21.1% of secondary sulfate during clean, transition, and polluted periods, respectively.	(Huang et al., 2019b)
Global Chemical Transport Model (GEOS-Chem)	The main aqueous oxidants were assumed to facilitate sulfate formation on aerosol surfaces, and the revised presents approximately 20% of secondary sulfate from the heterogeneous reactions, with TMI-related pathways being the dominate one.	(Shao et al., 2019)
Atmospheric Mineral Aerosol Reaction (AMAR) model	Atmospheric sulfate formation is significantly (>50%) attributed to the photocatalytic effects of airborne mineral dust surfaces.	(Yu et al., 2017; Yu and Jang, 2018; Yu et al., 2020)
Weather Research and Forecasting model coupled with Chemistry (WRF-Chem)	The revised including the heterogeneous oxidation of SO_2 by O_2 catalyzed by Fe^{3+} successfully reproduced the sulfate formation in Beijing and Xi'an, China.	(Li et al., 2017b)
Observation-based model for Secondary Inorganic Aerosol (OBM-SIA)	During a typical haze-fog event in China, heterogeneous contribution reaches up to 30.6% during nighttime and 19.4% during daytime.	(Xue et al., 2016)
WRF-Chem	Doubling SO_2 emissions did not significantly affect sulfate concentrations, but adding heterogeneous oxidation of dissolved SO_2 by NO_2 substantially improved simulations of sulfate and other inorganic aerosols.	(Gao et al., 2016)
Weather Research and Forecasting–Community Multi-scale Air Quality (WRF-CMAQ) model	The revised CMAQ with heterogeneous chemistry ($\gamma \geq 2 \times 10^{-5}$) not only captures the magnitude and temporal variation of sulfate, but also reproduces the enhancement of relative contribution o sulfate to $PM_{2.5}$ mass from clean days to polluted haze days.	(Zheng et al., 2015)
CMAQ	Supported by the laboratory work on the heterogeneous reaction of SO_2 on ATD in the presence of coexisted gases (NH_3 and NO_2) and alternative RHs, the model performance advances by 6.6% in the simulation of wintertime sulfate concentrations in Beijing. To summary, heterogeneous chemistry contributed up to 23% of secondary sulfate.	(Zhang et al., 2019a)

Table S1-Continued.

Model description	Summary of key results	Reference
GEOS-Chem	Heterogeneous uptake of SO_2 on deliquesced aerosols was proposed to be an additional sulfate formation pathway and considering this process in the model results in a 70% increase of sulfate enhancement ratio (mean concentrations during the haze divided by those during the clean period) and a 120% increase in sulfate fraction in $PM_{2.5}$.	(Wang et al., 2014)
GEOS-Chem	The model simulation results were improved after considering the RH-dependent parameterization for uptake coefficients of SO_2, and the contribution of heterogeneous reactions to sulfate formation is 20-30% over North China.	(Tian et al., 2021)

Table S2. Laboratory experiments on the heterogeneous reaction of SO_2 on airborne dust particles.
(The references are listed by the order of publication year, with the newest one presented at the forefront.)

Studied particles	Main techniques	Summary of key results	Reference
Airborne clay minerals, prepared natural dust	DRIFTS	Driving factors and driving force of the dust-driven heterogeneous oxidation of SO_2, and the comparisons among diverse pathways in forming secondary sulfate aerosols.	This study
Natural volcanic and desert dusts	Flow reaction system, HPLC	Higher amounts of sulfites are positively correlated with the (Fe+Ti)/Si parameter, while higher amounts of sulfates are positively correlated to the amount of Na on the surface of dust.	(Urupina et al., 2022)
Natural volcanic samples and desert mineral dust samples	Flow reaction system	The behavior of natural dust sample cannot be typified by the oxides mixed by its mineral composition.	(Urupina et al., 2021)
Volcanic dust (Hagavatn) and sand dust (Gobi Desert Dust)	Flow reaction system, HPLC	A reversed-phase HPLC method was successfully developed for the assay of sulfites and sulfates on dust surfaces.	(Urupina et al., 2020)
Illite, nontronite, smectite, Arizona test dust	DRIFTS	Simulated cloud processing modifies iron speciation of the mineral dust and enhances the heterogeneous uptake of SO_2.	(Wang et al., 2019a)
Natural volcanic dusts (Mýrdalssandur, Dyngjusandur, Hagavatn, Maelifellsandur, Eyjafjallajökull)	Flow reaction system, DRIFTS	Uptake of SO_2 on natural volcanic dusts: kinetics and mechanism	(Urupina et al., 2019)
Arizona test dust	Flow tube reactor	A hindering-then-accelerating feature in the SO_2 uptake profile was observed on nitrate-containing ATD. The acceleration of SO_2 is mainly attributed to the accumulation of protons from SO_2 oxidation during the induction period.	(Zhang et al., 2019b)
Arizona test dust	Flow tube reactor	A new parameterization method was developed to describe the RH-dependent uptake coefficients for the heterogeneous reaction of SO_2 on ATD coexisted with NO_2 and NH_3.	(Zhang et al., 2019a)
Gobi desert dust, Arizona test dust	Indoor and outdoor chamber	Heterogeneous reaction of SO_2 influenced by the absence/presence of mineral dust particles, UV light, water vapor, O_3 and NO_x	(Park et al., 2017)
Volcanic glass and ash (trachybasalt, andesite, dacite, rhyolite, Eyjafjallajökull, Tungurahua, Pinatubo, Chaitén)	Knudsen flow reactor	Synergistic effects between the heterogeneous uptake of SO_2 and O_3 on volcanic glass and ash	(Maters et al., 2017)
Arizona test dust	Smog chamber system	Heterogeneous oxidation of SO_2 influenced by the presence of UV and diverse atmospheric oxidants	(Park and Jang, 2016)
Asian mineral dust, Tengger Desert dust, Arizona test dust	Filter-based flow reactor	Effects of moisture and H_2O_2 on the heterogeneous reaction of SO_2 on authentic dusts	(Huang et al., 2015)

Table S2-Continued.

Studied particles	Main techniques	Summary of key results	Reference
Inner Mongolia desert dust, Xinjiang sierozem	Knudsen cell, smog chamber system	Kinetics evaluation, temperature dependence and moisture dependence	(Zhou et al., 2014)
Saharan dust	Filter-based flow reactor	Measurements of the stable isotope fractionation of $^{34}S/^{32}S$ during the heterogeneous oxidation on dust surfaces and aqueous oxidation in dust leachate.	(Harris et al., 2012)
Asian dust storm particles	Knudsen cell/MS	Morphology, elemental fraction, source distribution, uptake coefficients, and hygroscopic behavior	(Ma et al., 2012)
Saharan dust	Flow tube system	Uptake kinetics influenced by initial SO_2 concentration, flow conditions, temperature and relative humidity	(Adams et al., 2005)
Saharan dust	DRIFTS, Knudsen cell	There is no significant difference in uptake when SO_2 or NO_2 were introduced individually compared to experiments in which SO_2 and NO_2 were present at the same time.	(Ullerstam et al., 2003)
China loess	FTIR, Knudsen cell	The kinetics of Chinese loess can be predicted from the reactivities of the mineral components therein along with their natural abundances.	(Usher et al., 2002)
Saharan dust	DRIFTS	Effects of O_3 and water vapor on the heterogeneous reaction of SO_2 on mineral dust	(Ullerstam et al., 2002)

Table S3. Parameters for determining the Henry's law constants.

Equilibrium	Symbol	H_{298K} (M atm^{-1})	$-\Delta H_{298K}/R$ (K)	Reference
$SO_2(g) \leftrightharpoons SO_2(aq)$	H_{SO2}	1.23	3145.3	(Cheng et al., 2016; Seinfeld and Pandis, 2016)
$H_2O_2(g) \leftrightharpoons H_2O_2(aq)$	H_{H2O2}	100000	7297.1	(Cheng et al., 2016; Seinfeld and Pandis, 2016)
$O_3(g) \leftrightharpoons O_3(aq)$	H_{O3}	0.011	2536.4	(Cheng et al., 2016; Seinfeld and Pandis, 2016)
$NO_2(g) \leftrightharpoons NO_2(aq)$	H_{NO2}	0.01	2516.2	(Cheng et al., 2016; Seinfeld and Pandis, 2016)
$HOCl(g) \leftrightharpoons HOCl(aq)$	H_{HOCl}	650	5900	(Burkholder et al., 2015; Sander, 2015; Liu and Abbatt, 2020)
$HOBr(g) \leftrightharpoons HOBr(aq)$[a]	H_{HOBr}	343	—	(Blatchley et al., 1992)
$CH_3OOH(g) \leftrightharpoons CH_3OOH(aq)$	H_{CH3OOH}	310	5586.0	(Lind and Kok, 1986; Seinfeld and Pandis, 2016)
$CH_3COOOH(g) \leftrightharpoons CH_3COOOH(aq)$	$H_{CH3COOOH}$	473	6139.6	(Lind and Kok, 1986; Seinfeld and Pandis, 2016)
$HONO(g) \leftrightharpoons HONO(aq)$	H_{HONO}	49	4882.0	(Park and Lee, 1988)
$HO_2NO_2(g) \leftrightharpoons HO_2NO_2(aq)$[c]	H_{HNO4}	12600	6867.9	(Régimbal and Mozurkewich, 1997; Zhang et al., 1997; Berglen et al., 2004)

a $H_{HOBr}=1/2H_{HOCl}$

Table S4. Parameterization for the estimation of mass transfer rate coefficient (k_{MT}) under the experimental temperature (296.8 K).

	D_g ($\times 10^{-5}$ m^2 s^{-1})	α	v (m s^{-1})	Reference
SO_2	1.24	0.14	313.3	(Worsnop et al., 1989; Boniface et al., 2000)
H_2O_2	1.53	0.10	429.9	(Worsnop et al., 1989)
O_3	1.78	0.01	361.8	(Burkholder et al., 2015)
NO_2[a]	1.40	0.0002	369.6	(Mertes and Wahner, 1995; Jacob, 2000; Cheng et al., 2016)
HONO	1.27	0.05	365.6	(Bongartz et al., 1994; Jacob, 2000; Liu et al., 2021)
HO_2NO_2	1.44	0.01	282.0	(Warneck, 1999)
HOCl	1.49	0.8	346.0	(Hanson and Lovejoy, 1996)
HOBr	1.11	0.6	254.5	(Wachsmuth et al., 2002)
CH_3OOH	1.39	0.0048	361.8	(Magi et al., 1997)
CH_3COOOH[b]	1.08	0.0048	287.5	—

[a] The α was experimentally determined below normal room temperature (~ 298 K).
[b] The mass accommodation of CH_3COOOH is not available and assumed to be equivalent to that of CH_3OOH.

Table S5. Atmospheric oxidant concentrations for the sulfate formation rate calculations.

oxidant (unit)	concentration/mixing ratio		Reference
	nighttime	daytime	
OH (10^6 molecule cm^{-3})	0.7	7	(Lu et al., 2013; Tan et al., 2019; Feng et al., 2021; Wei et al., 2021)
stabilized CIs (10^4 molecule cm^{-3}) [a]	10	2	(Novelli et al., 2017; Liu et al., 2019; Cox et al., 2020)
NO_3 (ppt)	20	—	(Wang et al., 2015b; Wang et al., 2018)
O_3 (ppb)	10	80	(Jia et al., 2020; Zhang et al., 2020)
H_2O_2 (ppb)	0.2	2	(He et al., 2010; Zhang et al., 2010; Zhang et al., 2012a; Qin et al., 2018)
CH_3OOH (ppb)	0.1	0.6	(He et al., 2010; Zhang et al., 2010; Zhang et al., 2012a; Qin et al., 2018)
CH_3COOOH (ppb)	0.02	0.1	(He et al., 2010; Zhang et al., 2010; Qin et al., 2018)
NO_2 (ppb)	35	10	(Jia et al., 2020; Zhang et al., 2020)
HONO (ppb)	4	1	(Jia et al., 2020; Zhang et al., 2020)
HO_2NO_2 (ppt) [b]	5	—	(Dentener et al., 2002; Berglen et al., 2004; Tilgner et al., 2021)
HOCl (ppt) [c]	0.065	6.5	(Liu et al., 2017; Wang et al., 2019b; Li et al., 2021)
HOBr (ppt) [c]	0.025	2.5	(Liao et al., 2012; Zhu et al., 2019; Li et al., 2021)
T* (10^{-10} M)	—	1.6	(Wang et al., 2020)
airborne dust (μg m^{-3})	55	55	(Zhang et al., 2012b)

a The concentrations of stabilized CIs were averaged to be ~ 6×10^4 molecules cm^{-3} during the warm season in Beijing-Tianjin-Hebei (BTH) region, China. The dominate peak concentrations of sCI were frequently observed in the absence or limited sunlight irradiation.

b The nocturnal concentration was measured in the cold season, and the diurnal level is negligible due to the photolysis process.

c The concentrations of HOCl and HOBr decrease to near zero in the absence of sunlight and were assumed to be the 1% of the daytime concentrations.

Table S6. Element composition (wt%) of the airborne clay minerals derived by XRF

	NAu	CCa	SWy	KGa	IMt
Oxygen (O)	43.32	46.72	49.16	49.98	46.31
Silicon (Si)	25.66	19.09	31.55	26.57	27.80
Aluminum (Al)	1.49	11.54	10.20	19.85	10.31
Iron (Fe)	27.32	1.72	4.13	1.38	5.60
Calcium (Ca)	1.04	0.03	1.26	0.01	0.26
Sodium (Na)	0.14	0.01	0.96	0.00	0.06
Potassium (K)	0.12	0.05	0.64	0.05	7.24
Magnesium (Mg)	0.57	20.68	1.85	0.02	1.45
Titanium (Ti)	0.14	0.14	0.13	2.06	0.59
Manganese (Mn)	0.00	0.02	0.02	0.00	0.02
Total	**99.79**	**99.98**	**99.91**	**99.91**	**99.65**

Table S7. Assignments for the sulfur-bearing species formed on the clay minerals and natural dust observed by DRIFTS.

		NAu	CCa	SWy	KGa	IMt	natural dust
DARK	Hydrated SO_2	1147, 1125	1125	1151	1116	1047	1144, 1123
	Bisulfite	1089	1074	1075	--	1080	1078
	Sulfite	1000-700; 1063 (NAu); 1052 (CCa); 1048, 1025, 1006 (SWy); 1032 (KGa)					
	Coordinated sulfate	1246, 1215, 1179, 1164, 1201	1258, 1203, 1169, 1086	1257, 1203	1163	1190	1181
	Solvated sulfate	1106	1103	1108	1092	1099	1110, 1095
	Bisulfate	--	1229	1233	--	1234	1240
LIGHT	Hydrated SO_2	1131	1142	1155	1121	1049	1148, 1124
	Bisulfite	1076	1075	1077	--	1080	1074
	Sulfite	1000-700; 1059 (NAu); 1048 (CCa)					
	Coordinated sulfate	1249, 1198, 1180, 1161	1257, 1192	1256, 1191, 1110	1170	1195	1187
	Solvated sulfate	1104	1109	1100	1096	1101	1112, 1094
	Bisulfate	--	--	1225	1212	1237	1232

Table S8. Reactive uptake coefficients (γ) for the heterogeneous formation of sulfate on the clay minerals and the corresponding particle acidity (pH) after SO_2 exposure.

		Dark	Light
Reactive uptake coefficient, γ (× 10^5)	NAu	0.93±0.12	0.47±0.07
	CCa	0.49±0.09	0.74±0.15
	SWy	1.14±0.08	1.15±0.10
	KGa	0.12±0.02	0.36±0.03
	IMt	0.53±0.07	1.22±0.10
Particle acidity (pH)	NAu	4.56±0.19	5.37±0.25
	CCa	3.38±0.21	3.27±0.15
	SWy	5.08±0.12	4.85±0.14
	KGa	4.49±0.25	4.33±0.11
	IMt	4.21±0.18	4.01±0.11

References

Adams, J. W., Rodriguez, D., and Cox, R. A.: The uptake of SO_2 on Saharan dust: a flow tube study, Atmos. Chem. Phys., 5, 2679-2689, https://doi.org/10.5194/acpd-5-2643-2005, 2005.

Alexander, B., Park, R. J., Jacob, D. J., and Gong, S.: Transition metal-catalyzed oxidation of atmospheric sulfur: Global implications for the sulfur budget, J. Geophys. Res., 114, D2309, https://doi.org/10.1029/2008JD010486, 2009.

Ali, H. M., Iedema, M., Yu, X. Y., and Cowin, J. P.: Ionic strength dependence of the oxidation of SO_2 by H_2O_2 in sodium chloride particles, Atmos. Environ., 89, 731-738, https://doi.org/10.1016/j.atmosenv.2014.02.045, 2014.

Berglen, T. F., Berntsen, T. K., Isaksen, I. S. A., and Sundet, J. K.: A global model of the coupled sulfur/oxidant chemistry in the troposphere: The sulfur cycle, J. Geophys. Res., 109, D19310, https://doi.org/10.1029/2003JD003948, 2004.

Bian, H., and Zender, C. S.: Mineral dust and global tropospheric chemistry: Relative roles of photolysis and heterogeneous uptake, J. Geophys. Res.: Atmos., 108, 4672, https://doi.org/10.1029/2002JD003143, 2003.

Blatchley, E. R., Johnson, R. W., Alleman, J. E., and McCoy, W. F.: Effective Henry's law constants for free chlorine and free bromine, Water Res., 26, 99-106, https://doi.org/10.1016/0043-1354(92)90117-M, 1992.

Bongartz, A., Kames, J., Schurath, U., George, C., Mirabel, P., and Ponche, J. L.: Experimental determination of HONO mass accommodation coefficients using two different techniques, J. Atmos. Chem., 18, 149-169, https://doi.org/10.1007/BF00696812, 1994.

Boniface, J., Shi, Q., Li, Y. Q., Cheung, J. L., Rattigan, O. V., Davidovits, P., Worsnop, D. R., Jayne, J. T., and Kolb, C. E.: Uptake of Gas-Phase SO_2, H_2S, and CO_2 by Aqueous Solutions, J. Phys. Chem. A, 104, 7502-7510, https://doi.org/10.1021/jp000479h, 2000.

Burkholder, J. B., Sander, S. P., Abbatt, J., Barker, J. R., Huie, R. E., Kolb, C. E., Kurylo, M. J., Orkin, V. L., Wilmouth, D. M., and Wine, P. H.: Chemical Kinetics and Photochemical Data for Use in Atmospheric Studies Evaluation Number 18, https://doi.org/10.13140/RG.2.1.2504.2806, 2015.

Chen, Y., Tong, S., Li, W., Liu, Y., Tan, F., Ge, M., Xie, X., and Sun, J.: Photocatalytic Oxidation of SO_2 by TiO_2: Aerosol Formation and the Key Role of Gaseous Reactive Oxygen Species, Environ. Sci. Technol., 55, 9784-9793, https://doi.org/10.1021/acs.est.1c01608, 2021.

Chen, Z., Liu, P., Wang, W., Cao, X., Liu, Y., Zhang, Y., and Ge, M.: Rapid Sulfate Formation via Uncatalyzed Autoxidation of Sulfur Dioxide in Aerosol Microdroplets, Environ. Sci. Technol., 56, 7637-7646, https://doi.org/10.1021/acs.est.2c00112, 2022.

Cheng, Y., Zheng, G., Wei, C., Mu, Q., Zheng, B., Wang, Z., Gao, M., Zhang, Q., He, K., Carmichael, G., Pöschl, U., and Su, H.: Reactive nitrogen chemistry in aerosol water as a source of sulfate during haze events in China, Sci. Adv., 2, e1601530, https://doi.org/10.1126/sciadv.1601530, 2016.

Clifton, C. L., Altstein, M., and Hule, R. E.: Rate Constant for the Reaction of NO_2 with Sulfur(IV) over the pH Range 5.3-13, Environ. Sci. Technol., 22, 586-589, https://doi.org/10.1021/es00170a018, 1988.

Cox, R. A., Ammann, M., Crowley, J. N., Herrmann, H., Jenkin, M. E., McNeill, V. F., Mellouki, A., Troe, J., and Wallington, T. J.: Evaluated kinetic and photochemical data for atmospheric chemistry: Volume VII – Criegee intermediates, Atmos. Chem. Phys., 20, 13497-13519, https://doi.org/10.5194/acp-20-13497-2020, 2020.

Crowley, J. N., Ammann, M., Cox, R. A., Hynes, R. G., Jenkin, M. E., Mellouki, A., Rossi, M. J., Troe, J., and Wallington, T. J.: Evaluated kinetic and photochemical data for atmospheric chemistry: Volume V – heterogeneous reactions on solid substrates, Atmos. Chem. Phys., 10, 9059-9223, https://doi.org/10.5194/acp-10-9059-2010, 2010.

Dentener, F., Williams, J., and Metzger, S.: Aqueous Phase Reaction of HNO_4: The Impact on Tropospheric Chemistry, J. Atmos. Chem., 41, 109-133, https://doi.org/10.1023/A:1014233910126, 2002.

Ding, J., Zhao, P., Su, J., Dong, Q., Du, X., and Zhang, Y.: Aerosol pH and its driving factors in Beijing, Atmos. Chem. Phys., 19, 7939-7954, https://doi.org/10.5194/acp-19-7939-2019, 2019.

Dupart, Y., King, S. M., Nekat, B., Nowak, A., Wiedensohler, A., Herrmann, H., David, G., Thomas, B., Miffre, A., Rairoux, P., Anna, B. D., and George, C.: Mineral dust photochemistry induces nucleation events in the presence of SO_2, P. Natl. Acad. Sci. USA, 109, 20842-20847, https://doi.org/10.1073/pnas.1212297109, 2012.

Feng, T., Zhao, S., Hu, B., Bei, N., Zhang, X., Wu, J., Li, X., Liu, L., Wang, R., Tie, X., and Li, G.: Assessment of Atmospheric Oxidizing Capacity Over the Beijing-Tianjin-Hebei (BTH) Area, China, J. Geophys. Res.: Atmos., 126, https://doi.org/10.1029/2020JD033834, 2021.

Fuller, E. N., Ensley, K., and Giddings, J. C.: Diffusion of halogenated hydrocarbons in helium. The effect of structure on collision cross sections, J. Phys. Chem., 73, 3679-3685, https://doi.org/10.1021/j100845a020, 1969.

Gao, M., Carmichael, G. R., Wang, Y., Ji, D., Liu, Z., and Wang, Z.: Improving simulations of sulfate aerosols during winter haze over Northern China: the impacts of heterogeneous oxidation by NO_2, Front. Env. Sci. Eng., 10, https://doi.org/10.1007/s11783-016-0878-2, 2016.

Gen, M., Zhang, R., Huang, D. D., Li, Y., and Chan, C. K.: Heterogeneous SO_2 Oxidation in Sulfate Formation by Photolysis of Particulate Nitrate, Environ. Sci. Technol. Lett., 6, 86-91, https://doi.org/10.1021/acs.estlett.8b00681, 2019b.

Gen, M., Zhang, R., Huang, D., Li, Y., and Chan, C. K.: Heterogeneous Oxidation of SO_2 in Sulfate Production during Nitrate Photolysis at 300 nm: Effect of pH, Relative Humidity, Irradiation Intensity, and the Presence of Organic Compounds, Environ. Sci. Technol., 53, 8757-8766, https://doi.org/10.1021/acs.est.9b01623, 2019a.

Hanson, D. R., and Lovejoy, E. R.: Heterogeneous Reactions in Liquid Sulfuric Acid: HOCl+HCl as a Model System, J. Phys. Chem., 100, 6397-6405, https://doi.org/10.1021/jp953250o, 1996.

Harris, E., Sinha, B., Foley, S., Crowley, J. N., Borrmann, S., and Hoppe, P.: Sulfur isotope fractionation during heterogeneous oxidation of SO_2 on mineral dust, Atmos. Chem. Phys., 12, 4867-4884, https://doi.org/10.5194/acp-12-4867-2012, 2012.

He, S. Z., Chen, Z. M., Zhang, X., Zhao, Y., Huang, D. M., Zhao, J. N., Zhu, T., Hu, M., and Zeng, L. M.: Measurement of atmospheric hydrogen peroxide and organic peroxides in Beijing before and during the 2008 Olympic Games: Chemical and physical factors influencing their concentrations, J. Geophys. Res., 115, https://doi.org/10.1029/2009JD013544, 2010.

Huang, L., An, J., Koo, B., Yarwood, G., Yan, R., Wang, Y., Huang, C., and Li, L.: Sulfate formation during heavy winter haze events and the potential contribution from heterogeneous SO_2+NO_2 reactions in the Yangtze River Delta region, China, Atmos. Chem. Phys., 19, 14311-14328, https://doi.org/10.5194/acp-19-14311-2019, 2019a.

Huang, L., An, J., Koo, B., Yarwood, G., Yan, R., Wang, Y., Huang, C., and Li, L.: Enhanced sulfate formation through SO_2+NO_2 heterogeneous reactions during heavy winter haze in the Yangtze River Delta region, China, Atmos. Chem. Phys., 19, 14311-14328, https://doi.org/10.5194/acp-2019-292, 2019b.

Huang, L., Zhao, Y., Li, H., and Chen, Z.: Kinetics of heterogeneous reaction of sulfur dioxide on authentic mineral dust: effects of relative humidity and hydrogen peroxide, Environ. Sci. Technol., 49, 10797-10805, https://doi.org/10.1021/acs.est.5b03930, 2015.

Hung, H., Hsu, M., and Hoffmann, M. R.: Quantification of SO_2 Oxidation on Interfacial Surfaces of Acidic Micro-Droplets: Implication for Ambient Sulfate Formation, Environ. Sci. Technol., 52, 9079-9086, https://doi.org/10.1021/acs.est.8b01391, 2018.

Hung, H., and Hoffmann, M. R.: Oxidation of Gas-Phase SO_2 on the Surfaces of Acidic Microdroplets: Implications for Sulfate and Sulfate Radical Anion Formation in the Atmospheric Liquid Phase, Environ. Sci. Technol., 49, 13768-13776, https://doi.org/10.1021/acs.est.5b01658, 2015.

Ibusuki, T., and Takeuchi, K.: Sulfur Dioxide Oxidation by Oxygen Catalyzed by Mixtures of Manganese(II) and Iron(III) in Aqueous Solutions at Environmental Reaction Conditions, Atmos. Environ., 21, 1555-1560, https://doi.org/10.1016/0004-6981(87)90317-9, 1987.

Jacob, D. J.: Heterogeneous chemistry and tropospheric ozone, Atmos. Environ., 34, 2131-2159, https://doi.org/10.1016/S1352-2310(99)00462-8, 2000.

Jankowski, J. J., Kieber, D. J., Mopper, K., and Neale, P. J.: Development and intercalibration of ultraviolet solar actinometers, Photochem. Photobiol., 71, 431-440, https://doi.org/10.1562/0031-8655(2000)071<0431:daious>2.0.co;2, 2000.

Jayne, J. T., Dum, S. X., Davidovits, P., Wonnop, D. R., Zahniser, M. S., and Kolb, C. E.: Uptake of Gas-Phase Alcohol and Organic Acid Molecules by Water Surfaces, J. Phys. Chem., 95, 6329-6336, https://doi.org/10.1021/j100169a047, 1991.

Jia, C., Tong, S., Zhang, W., Zhang, X., Li, W., Wang, Z., Wang, L., Liu, Z., Hu, B., Zhao, P., and Ge, M.: Pollution characteristics and potential sources of nitrous acid (HONO) in early autumn 2018 of Beijing, Sci. Total Environ., 735, 139317, https://doi.org/10.1016/j.scitotenv.2020.139317, 2020.

Kosak-Channing, L. F., and Helz, G. R.: Solubility of ozone in aqueous solutions of 0-0.6 M ionic strength at 5-30°C, Environ. Sci. Technol., 17, 145-149, https://doi.org/10.1021/es00109a005, 1983.

Kumar, R., Barth, M. C., Madronich, S., Naja, M., Carmichael, G. R., Pfister, G. G., Knote, C., Brasseur,

G. P., Ojha, N., and Sarangi, T.: Effects of dust aerosols on tropospheric chemistry during a typical pre-monsoon season dust storm in northern India, Atmos. Chem. Phys., 14, 6813-6834, https://doi.org/10.5194/acp-14-6813-2014, 2014.

Lagrange, J., Pallares, C., and Lagrang, P.: Electrolyte effects on aqueous atmospheric oxidation of sulphur dioxide by ozone, J. Geophys. Res., 99, 14595-14600, https://doi.org/10.1016/0960-1686(93)90342-V, 1994.

Li, G., Bei, N., Cao, J., Huang, R., and Wu, J.: A possible pathway for rapid growth of sulfate during haze days in China, Atmos. Chem. Phys., 17, 3301-3316, https://doi.org/10.5194/acp-17-3301-2017, 2017b.

Li, M., Wang, T., Han, Y., Xie, M., Li, S., Zhuang, B., and Chen, P.: Modeling of a severe dust event and its impacts on ozone photochemistry over the downstream Nanjing megacity of eastern China, Atmos. Environ., 160, 107-123, https://doi.org/10.1016/j.atmosenv.2017.04.010, 2017a.

Li, Q., Fu, X., Peng, X., Wang, W., Badia, A., Fernandez, R. P., Cuevas, C. A., Mu, Y., Chen, J., Jimenez, J. L., Wang, T., and Saiz-Lopez, A.: Halogens Enhance Haze Pollution in China, Environ. Sci. Technol., 55, 13625-13637, https://doi.org/10.1021/acs.est.1c01949, 2021.

Li, X., Wang, L., Ji, D., Wen, T., Pan, Y., Sun, Y., and Wang, Y.: Characterization of the size-segregated water-soluble inorganic ions in the Jing-Jin-Ji urban agglomeration: Spatial/temporal variability, size distribution and sources, Atmos. Environ., 77, 250-259, https://doi.org/10.1016/j.atmosenv.2013.03.042, 2013.

Liao, J., Huey, L. G., Tanner, D. J., Flocke, F. M., Orlando, J. J., Neuman, J. A., Nowak, J. B., Weinheimer, A. J., Hall, S. R., Smith, J. N., Fried, A., Staebler, R. M., Wang, Y., Koo, J. H., Cantrell, C. A., Weibring, P., Walega, J., Knapp, D. J., Shepson, P. B., and Stephens, C. R.: Observations of inorganic bromine (HOBr, BrO, and Br_2) speciation at Barrow, Alaska, in spring 2009, J. Geophys. Res., 117, D16R, https://doi.org/10.1029/2011JD016641, 2012.

Lind, J. A., Lazrus, A. L., and Kok, G. L.: Aqueous phase oxidation of sulfur(IV) by hydrogen peroxide, methylhydroperoxide, and peroxyacetic acid, J. Geophys. Res., 92, 4171-4177, https://doi.org/10.1029/JD092iD04p04171, 1987.

Lind, J., and Kok, G.: Henry's Law Determinations for Aqueous Solutions of Hydrogen Peroxide, Methylhydroperoxide, and Peroxyacetic Acid, J. Geophys. Res., 91, 7889-7895, https://doi.org/10.1029/jd091id07p07889, 1986.

Liu, L., Bei, N., Wu, J., Liu, S., Zhou, J., Li, X., Yang, Q., Feng, T., Cao, J., Tie, X., and Li, G.: Effects of stabilized Criegee intermediates (sCIs) on sulfate formation: a sensitivity analysis during summertime in Beijing–Tianjin–Hebei (BTH), China, Atmos. Chem. Phys., 19, 13341-13354, https://doi.org/10.5194/acp-19-13341-2019, 2019.

Liu, T., Chan, A. W. H., and Abbatt, J. P. D.: Multiphase Oxidation of Sulfur Dioxide in Aerosol Particles: Implications for Sulfate Formation in Polluted Environments, Environ. Sci. Technol., 55, 4227-4242, https://doi.org/10.1021/acs.est.0c06496, 2021.

Liu, T., Clegg, S. L., and Abbatt, J. P. D.: Fast oxidation of sulfur dioxide by hydrogen peroxide in deliquesced aerosol particles, P. Natl. Acad. Sci. USA, 117, 1354-1359, https://doi.org/10.1073/pnas.1916401117, 2020.

Liu, T., and Abbatt, J. P. D.: An Experimental Assessment of the Importance of S(IV) Oxidation by Hypohalous Acids in the Marine Atmosphere, Geophys. Res. Lett., 47, e2019G-e86465G, https://doi.org/10.1029/2019GL086465, 2020.

Liu, T., and Abbatt, J. P. D.: Oxidation of sulfur dioxide by nitrogen dioxide accelerated at the interface of deliquesced aerosol particles, Nat. Chem., 13, 1173-1177, https://doi.org/10.1038/s41557-021-00777-0, 2021.

Liu, X., Qu, H., Huey, L. G., Wang, Y., Sjostedt, S., Zeng, L., Lu, K., Wu, Y., Hu, M., Shao, M., Zhu, T., and Zhang, Y.: High Levels of Daytime Molecular Chlorine and Nitryl Chloride at a Rural Site on the North China Plain, Environ. Sci. Technol., 51, 9588-9595, https://doi.org/10.1021/acs.est.7b03039, 2017.

Lu, K. D., Hofzumahaus, A., Holland, F., Bohn, B., Brauers, T., Fuchs, H., Hu, M., Häseler, R., Kita, K., Kondo, Y., Li, X., Lou, S. R., Oebel, A., Shao, M., Zeng, L. M., Wahner, A., Zhu, T., Zhang, Y. H., and Rohrer, F.: Missing OH source in a suburban environment near Beijing: observed and modelled OH and HO_2 concentrations in summer 2006, Atmos. Chem. Phys., 13, 1057-1080, https://doi.org/10.5194/acp-13-1057-2013, 2013.

Ma, Q., Liu, Y., Liu, C., Ma, J., and He, H.: A case study of Asian dust storm particles: Chemical composition, reactivity to SO_2 and hygroscopic properties, J. Environ. Sci.-China, 24, 62-71, https://doi.org/10.1016/S1001-0742(11)60729-8, 2012.

Maahs, H. G.: Kinetics and Mechanism of the Oxidation of S(IV) by Ozone in Aqueous Solution With

Particular Reference to SO_2 Conversion in Nonurban Tropospheric Clouds, J. Geophys. Res., 88, 10721-10732, https://doi.org/10.1029/JC088iC15p10721, 1983.
Maaβ, F., Elias, H., and Wannowius, K. J.: Kinetics of the oxidation of hydrogen sulfite by hydrogen peroxide in aqueous solution: ionic strength effects and temperature dependence, Atmos. Environ., 33, 4413-4419, https://doi.org/10.1016/S1352-2310(99)00212-5, 1999.
Magi, L., Schweitzer, F., Pallares, C., Cherif, S., Mirabel, P., and George, C.: Investigation of the Uptake Rate of Ozone and Methyl Hydroperoxide by Water Surfaces, J. Phys. Chem. A, 101, 4943-4949, https://doi.org/10.1021/jp970646m, 1997.
Martin, L. R., and Hill, M. W.: The effect of ionic strength on the manganese catalyzed oxidation of sulfur(IV), Atmos. Environ., 21, 2267-2270, https://doi.org/10.1016/0004-6981(87)90361-1, 1987.
Maters, E. C., Delmelle, P., Rossi, M. J., and Ayris, P. M.: Reactive Uptake of Sulfur Dioxide and Ozone on Volcanic Glass and Ash at Ambient Temperature, J. Geophys. Res.: Atmos., 122, 10077-10088, https://doi.org/10.1002/2017JD026993, 2017.
Mauldin III, R. L., Berndt, T., Sipilä, M., Paasonen, P., Petäjä, T., Kim, S., Kurtén, T., Stratmann, F., Kerminen, V. M., and Kulmala, M.: A new atmospherically relevant oxidant of sulphur dioxide, Nature, 488, 193-196, https://doi.org/10.1038/nature11278, 2012.
McArdle, J. V., and Hoffmann, M. R.: Kinetics and mechanism of the oxidation of aquated sulfur dioxide by hydrogen peroxide at low pH, J. Phys. Chem., 87, 5425-5429, https://doi.org/10.1021/j150644a024, 1983.
Mertes, S., and Wahner, A.: Uptake of Nitrogen Dioxide and Nitrous Acid on Aqueous Surfaces, J. Phys. Chem., 99, 14000-14006, https://doi.org/10.1021/j100038a035, 1995.
Millero, F. J., Hershey, J. P., Johnson, G., and Zhang, J.: The Solubility of SO_2 and the Dissociation of H_2SO_3 in NaCl Solutions, J. Atmos. Chem., 8, 377-389, https://doi.org/10.1007/BF00052711, 1989.
Nair, S. K., and Peters, L. K.: Studies on non-precipitating cumulus cloud acidification, Atmos. Environ. (1967-1989), 23, 1399-1423, https://doi.org/10.1016/0004-6981(89)90162-5, 1989.
Novelli, A., Hens, K., Tatum Ernest, C., Martinez, M., Nölscher, A. C., Sinha, V., Paasonen, P., Petäjä, T., Sipilä, M., Elste, T., Plass-Dülmer, C., Phillips, G. J., Kubistin, D., Williams, J., Vereecken, L., Lelieveld, J., and Harder, H.: Estimating the atmospheric concentration of Criegee intermediates and their possible interference in a FAGE-LIF instrument, Atmos. Chem. Phys., 17, 7807-7826, https://doi.org/10.5194/acp-17-7807-2017, 2017.
Oblath, S. B., Markowitz, S. S., Novakov, T., and Chang, S. G.: Kinetics of the initial reaction of nitrite ion in bisulfite solutions, J. Phys. Chem., 86, 4853-4857, https://doi.org/10.1021/j100222a005, 1982.
Park, J. Y., and Lee, Y. N.: Solubility and decomposition kinetics of nitrous acid in aqueous solution, J. Phys. Chem., 92, 6294-6302, https://doi.org/10.1021/j100333a025, 1988.
Park, J., Jang, M., and Yu, Z.: Heterogeneous Photo-oxidation of SO_2 in the Presence of Two Different Mineral Dust Particles: Gobi and Arizona Dust, Environ. Sci. Technol., 51, 9605-9613, https://doi.org/10.1021/acs.est.7b00588, 2017.
Park, J., and Jang, M.: Heterogeneous photooxidation of sulfur dioxide in the presence of airborne mineral dust particles, RSC Adv., 6, 58617-58627, https://doi.org/10.1039/C6RA09601H, 2016.
Qin, M., Chen, Z., Shen, H., Li, H., Wu, H., and Wang, Y.: Impacts of heterogeneous reactions to atmospheric peroxides: Observations and budget analysis study, Atmos. Environ., 183, 144-153, https://doi.org/10.1016/j.atmosenv.2018.04.005, 2018.
Régimbal, J., and Mozurkewich, M.: Peroxynitric Acid Decay Mechanisms and Kinetics at Low pH, J. Phys. Chem. A, 101, 8822-8829, https://doi.org/10.1021/jp971908n, 1997.
Robbin Martin, L., and Hill, M. W.: The iron catalyzed oxidation of sulfur: Reconciliation of the literature rates, Atmos. Environ. (1967-1989), 21, 1487-1490, https://doi.org/10.1016/0004-6981(67)90100-X, 1967.
RobbinMartin, L., Damschen, D. E., and Judeikis, H. S.: The reactions of nitrogen oxides with SO_2 in aqueous aerosols, Atmos. Environ., 15, 191-195, https://doi.org/10.1016/0004-6981(81)90010-X, 1981.
Sander, R.: Compilation of Henry's law constants (version 4.0) for water as solvent, Atmos. Chem. Phys., 15, 4399-4981, https://doi.org/10.5194/acp-15-4399-2015, 2015.
Seinfeld, J. H., and Pandis, S. N.: Atmospheric Chemistry and Physics, From Air Pollution to Climate Change, 3rd Edition, Wiley, New Jersey, USA, 2016.
Shao, J., Chen, Q., Wang, Y., Lu, X., He, P., Sun, Y., Shah, V., Martin, R. V., Philip, S., Song, S., Zhao, Y., Xie, Z., Zhang, L., and Alexander, B.: Heterogeneous sulfate aerosol formation mechanisms during wintertime Chinese haze events: air quality model assessment using observations of sulfate oxygen isotopes in Beijing, Atmos. Chem. Phys., 19, 6107-6123, https://doi.org/10.5194/acp-19-6107-2019, 2019.

Shi, Q., Tao, Y., Krechmer, J. E., Heald, C. L., Murphy, J. G., Kroll, J. H., and Ye, Q.: Laboratory Investigation of Renoxification from the Photolysis of Inorganic Particulate Nitrate, Environ. Sci. Technol., 55, 854-861, https://doi.org/10.1021/acs.est.0c06049, 2021.

Sipilä, M., Berndt, T., Petäjä, T., Brus, D., Vanhanen, J., Stratmann, F., Patokoski, J., III, R. L. M., Hyvärinen, A., Lihavainen, H., and Kulmala, M.: The Role of Sulfuric Acid in Atmospheric Nucleation, Science, 327, 1243-1246, https://doi.org/10.1126/science.1180315, 2010.

Song, H., Lu, K., Ye, C., Dong, H., Li, S., Chen, S., Wu, Z., Zheng, M., Zeng, L., Hu, M., and Zhang, Y.: A comprehensive observation-based multiphase chemical model analysis of sulfur dioxide oxidations in both summer and winter, Atmos. Chem. Phys., 21, 13713-13727, https://doi.org/10.5194/acp-21-13713-2021, 2021.

Tan, Z., Lu, K., Jiang, M., Su, R., Wang, H., Lou, S., Fu, Q., Zhai, C., Tan, Q., Yue, D., Chen, D., Wang, Z., Xie, S., Zeng, L., and Zhang, Y.: Daytime atmospheric oxidation capacity in four Chinese megacities during the photochemically polluted season: a case study based on box model simulation, Atmos. Chem. Phys., 19, 3493-3513, https://doi.org/10.5194/acp-19-3493-2019, 2019.

Tang, M. J., Cox, R. A., and Kalberer, M.: Compilation and evaluation of gas phase diffusion coefficients of reactive trace gases in the atmosphere: volume 1. Inorganic compounds, Atmos. Chem. Phys., 14, 9233-9247, https://doi.org/10.5194/acp-14-9233-2014, 2014.

Tang, M., Huang, X., Lu, K., Ge, M., Li, Y., Cheng, P., Zhu, T., Ding, A., Zhang, Y., Gligorovski, S., Song, W., Ding, X., Bi, X., and Wang, X.: Heterogeneous reactions of mineral dust aerosol: implications for tropospheric oxidation capacity, Atmos. Chem. Phys., 17, 11727-11777, https://doi.org/10.5194/acp-17-11727-2017, 2017.

Tian, R., Ma, X., Sha, T., Pan, X., and Wang, Z.: Exploring dust heterogeneous chemistry over China: Insights from field observation and GEOS-Chem simulation, Sci. Total Environ., 798, 149307, https://doi.org/10.1016/j.scitotenv.2021.149307, 2021.

Tilgner, A., Schaefer, T., Alexander, B., Barth, M., Collett Jr., J. L., Fahey, K. M., Nenes, A., Pye, H. O. T., Herrmann, H., and McNeill, V. F.: Acidity and the multiphase chemistry of atmospheric aqueous particles and clouds, Atmos. Chem. Phys., 21, 13483-13536, https://doi.org/10.5194/acp-21-13483-2021, 2021.

Ullerstam, M., Johnson, M. S., Vogt, R., and Ljungstrom, E.: DRIFTS and Knudsen cell study of the heterogeneous reactivity of SO_2 and NO_2 on mineral dust, Atmos. Chem. Phys., 3, 2043-2051, https://doi.org/10.5194/acp-3-2043-2003, 2003.

Ullerstam, M., Vogt, R., Langer, S., and Ljungström, E.: The kinetics and mechanism of SO_2 oxidation by O_3 on mineral dust, Phys. Chem. Chem. Phys., 4, 4694-4699, https://doi.org/10.1039/B203529B, 2002.

Urupina, D., Gaudion, V., Romanias, M. N., Verriele, M., and Thevenet, F.: Method development and validation for the determination of sulfites and sulfates on the surface of mineral atmospheric samples using reverse-phase liquid chromatography, Talanta, 219, 121318, https://doi.org/10.1016/j.talanta.2020.121318, 2020.

Urupina, D., Gaudion, V., Romanias, M. N., and Thevenet, F.: Surface Distribution of Sulfites and Sulfates on Natural Volcanic and Desert Dusts: Impact of Humidity and Chemical Composition, ACS Earth Space Chem., 6, 642-655, https://doi.org/10.1021/acsearthspacechem.1c00321, 2022.

Urupina, D., Lasne, J., Romanias, M. N., Thiery, V., Dagsson-Waldhauserova, P., and Thevenet, F.: Uptake and surface chemistry of SO_2 on natural volcanic dusts, Atmos. Environ., 217, 116942, https://doi.org/10.1016/j.atmosenv.2019.116942, 2019.

Urupina, D., Romanias, M. N., and Thevenet, F.: How Relevant Is It to Use Mineral Proxies to Mimic the Atmospheric Reactivity of Natural Dust Samples? A Reactivity Study Using SO_2 as Probe Molecule, Minerals, 11, 282, https://doi.org/10.3390/min11030282, 2021.

Usher, C. R., Al-Hosney, H., Carlos-Cuellar, S., and Grassian, V. H.: A laboratory study of the heterogeneous uptake and oxidation of sulfur dioxide on mineral dust particles, J. Geophys. Res.: Atmos., 107, 4713, https://doi.org/10.1029/2002JD002051, 2002.

Wachsmuth, M., Gaggeler, H. W., von Glasow, R., and Ammann, M.: Accommodation coefficient of HOBr on deliquescent sodium bromide aerosol particles, Atmos. Chem. Phys., 2, 121-131, https://doi.org/10.5194/acpd-2-1-2002, 2002.

Walcek, C. J., and Taylor, G. R.: A Theoretical Method for Computing Vertical Distributions of Acidity and Sulfate Production within Cumulus Clouds, J. Atmos. Sci., 15, 339-355, https://doi.org/10.1175/1520-0469(1986)0432.0.CO;2, 1986.

Wang, D., Hu, R., Xie, P., Liu, J., Liu, W., Qin, M., Ling, L., Zeng, Y., Chen, H., Xing, X., Zhu, G., Wu, J., Duan, J., Lu, X., and Shen, L.: Diode laser cavity ring-down spectroscopy for in situ measurement of NO_3 radical in ambient air, J. Quant. Spectrosc. Radiat. Transfer, 166, 23-29,

https://doi.org/10.1016/j.jqsrt.2015.07.005, 2015b.
Wang, H., Lu, K., Guo, S., Wu, Z., Shang, D., Tan, Z., Wang, Y., Le Breton, M., Lou, S., Tang, M., Wu, Y., Zhu, W., Zheng, J., Zeng, L., Hallquist, M., Hu, M., and Zhang, Y.: Efficient N_2O_5 uptake and NO_3 oxidation in the outflow of urban Beijing, Atmos. Chem. Phys., 18, 9705-9721, https://doi.org/10.5194/acp-18-9705-2018, 2018.
Wang, K., Zhang, Y., Nenes, A., and Fountoukis, C.: Implementation of dust emission and chemistry into the Community Multiscale Air Quality modeling system and initial application to an Asian dust storm episode, Atmos. Chem. Phys., 12, 10209-10237, https://doi.org/10.5194/acp-12-10209-2012, 2012.
Wang, Q., Ma, Y., Tan, J., Zheng, N., Duan, J., Sun, Y., He, K., and Zhang, Y.: Characteristics of size-fractionated atmospheric metals and water-soluble metals in two typical episodes in Beijing, Atmos. Environ., 119, 294-303, https://doi.org/10.1016/j.atmosenv.2015.08.061, 2015a.
Wang, T., Liu, M., Liu, M., Song, Y., Xu, Z., Shang, F., Huang, X., Liao, W., Wang, W., Ge, M., Cao, J., Hu, J., Tang, G., Pan, Y., Hu, M., and Zhu, T.: Sulfate Formation Apportionment during Winter Haze Events in North China, Environ. Sci. Technol., 56, 7771-7778, https://doi.org/10.1021/acs.est.2c02533, 2022.
Wang, W., Liu, M., Wang, T., Song, Y., Zhou, L., Cao, J., Hu, J., Tang, G., Chen, Z., Li, Z., Xu, Z., Peng, C., Lian, C., Chen, Y., Pan, Y., Zhang, Y., Sun, Y., Li, W., Zhu, T., Tian, H., and Ge, M.: Sulfate formation is dominated by manganese-catalyzed oxidation of SO_2 on aerosol surfaces during haze events, Nat. Commun., 12, 1993, https://doi.org/10.1038/s41467-021-22091-6, 2021.
Wang, X., Gemayel, R., Hayeck, N., Perrier, S., Charbonnel, N., Xu, C., Chen, H., Zhu, C., Zhang, L., Wang, L., Nizkorodov, S. A., Wang, X., Wang, Z., Wang, T., Mellouki, A., Riva, M., Chen, J., and George, C.: Atmospheric Photosensitization: A New Pathway for Sulfate Formation, Environ. Sci. Technol., 54, 3114-3120, https://doi.org/10.1021/acs.est.9b06347, 2020.
Wang, X., Jacob, D. J., Eastham, S. D., Sulprizio, M. P., Zhu, L., Chen, Q., Alexander, B., Sherwen, T., Evans, M. J., Lee, B. H., Haskins, J. D., Lopez-Hilfiker, F. D., Thornton, J. A., Huey, G. L., and Liao, H.: The role of chlorine in global tropospheric chemistry, Atmos. Chem. Phys., 19, 3981-4003, https://doi.org/10.5194/acp-19-3981-2019, 2019b.
Wang, Y., Zhang, Q., Jiang, J., Zhou, W., Wang, B., He, K., Duan, F., Zhang, Q., Philip, S., and Xie, Y.: Enhanced sulfate formation during China's severe winter haze episode in January 2013 missing from current models, J. Geophys. Res., 119, 10425-10440, https://doi.org/10.1002/2013jd021426, 2014.
Wang, Z., Wang, T., Fu, H., Zhang, L., Tang, M., George, C., Grassian, V. H., and Chen, J.: Enhanced heterogeneous uptake of sulfur dioxide on mineral particles through modification of iron speciation during simulated cloud processing, Atmos. Chem. Phys., 19, 12569-12585, https://doi.org/10.5194/acp-19-12569-2019, 2019a.
Warneck, P.: The relative importance of various pathways for the oxidation of sulfur dioxide and nitrogen dioxide in sunlit continental fair weather clouds, Phys. Chem. Chem. Phys., 1, 5471-5483, https://doi.org/10.1039/A906558J, 1999.
Wei, W., Wang, Y., Bai, H., Wang, X., Cheng, S., and Wang, L.: Insights into atmospheric oxidation capacity and its impact on $PM_{2.5}$ in megacity Beijing via volatile organic compounds measurements, Atmos. Res., 258, 105632, https://doi.org/10.1016/j.atmosres.2021.105632, 2021.
Worsnop, D. R., Zahniser, M. S., Kolb, C. E., Gardner, J. A., Watson, L. R., Van Doren, J. M., Jayne, J. T., and Davidovits, P.: Temperature dependence of mass accommodation of SO_2 and H_2O_2 on aqueous surfaces, J. Phys. Chem., 93, 1159-1172, https://doi.org/10.1021/j100340a027, 1989.
Xie, Z. D.: Formation Mechanism of Condensation Nuclei in Nighttime Atmosphere and the Kinetics of the SO_2-O_3-NO_2 System, J. Phys. Chem., 96, 1543-1547, https://doi.org/10.1021/j100183a011, 1992.
Xue, J., Yuan, Z., Griffith, S. M., Yu, X., Lau, A. K. H., and Yu, J. Z.: Sulfate formation enhanced by a cocktail of high NO_x, SO_2, particulate matter, and droplet pH during haze-fog events in megacities in China: an observation-based modeling investigation, Environ. Sci. Technol., 50, 7325-7334, https://doi.org/10.1021/acs.est.6b00768, 2016.
Ye, C., Gao, H., Zhang, N., and Zhou, X.: Photolysis of Nitric Acid and Nitrate on Natural and Artificial Surfaces, Environ. Sci. Technol., 50, 3530-3536, https://doi.org/10.1021/acs.est.5b05032, 2016.
Yu, J.: An interfacial role for NO_2, Nat. Chem., 13, 1158-1160, https://doi.org/10.1038/s41557-021-00845-5, 2021.
Yu, Z., Jang, M., Kim, S., Bae, C., Koo, B., Beardsley, R., Park, J., Chang, L. S., Lee, H. C., Lim, Y., and Cho, J. H.: Simulating the Impact of Long-Range-Transported Asian Mineral Dust on the Formation of Sulfate and Nitrate during the KORUS-AQ Campaign, ACS Earth Space Chem., 4, 1039-1049, https://doi.org/10.1021/acsearthspacechem.0c00074, 2020.
Yu, Z., Jang, M., and Park, J.: Modeling atmospheric mineral aerosol chemistry to predict heterogeneous

photooxidation of SO_2, Atmos. Chem. Phys., 17, 10001-10017, https://doi.org/10.5194/acp-17-10001-2017, 2017.
Yu, Z., and Jang, M.: Simulation of heterogeneous photooxidation of SO_2 and NO_x in the presence of Gobi Desert dust particles under ambient sunlight, Atmos. Chem. Phys., 18, 14609-14622, https://doi.org/10.5194/acp-18-14609-2018, 2018.
Zhang, H., Xu, Y., and Jia, L.: A chamber study of catalytic oxidation of SO_2 by Mn^{2+}/Fe^{3+} in aerosol water, Atmos. Environ., 245, 118019, https://doi.org/10.1016/j.atmosenv.2020.118019, 2021.
Zhang, R., Leu, M., and Keyser, L. F.: Heterogeneous Chemistry of HO_2NO_2 in Liquid Sulfuric Acid, J. Phys. Chem. A, 101, 3324-3330, https://doi.org/10.1021/jp963321z, 1997.
Zhang, R., Sun, X., Shi, A., Huang, Y., Yan, J., Nie, T., Yan, X., and Li, X.: Secondary inorganic aerosols formation during haze episodes at an urban site in Beijing, China, Atmos. Environ., 177, 275-282, https://doi.org/10.1016/j.atmosenv.2017.12.031, 2018.
Zhang, S., Xing, J., Sarwar, G., Ge, Y., He, H., Duan, F., Zhao, Y., He, K., Zhu, L., and Chu, B.: Parameterization of heterogeneous reaction of SO_2 to sulfate on dust with coexistence of NH_3 and NO_2 under different humidity conditions, Atmos. Environ., 208, 133-140, https://doi.org/10.1016/j.atmosenv.2019.04.004, 2019a.
Zhang, W., Tong, S., Jia, C., Wang, L., Liu, B., Tang, G., Ji, D., Hu, B., Liu, Z., Li, W., Wang, Z., Liu, Y., Wang, Y., and Ge, M.: Different HONO Sources for Three Layers at the Urban Area of Beijing, Environ. Sci. Technol., 54, 12870-12880, https://doi.org/10.1021/acs.est.0c02146, 2020.
Zhang, X. Y., Wang, Y. Q., Niu, T., Zhang, X. C., Gong, S. L., Zhang, Y. M., and Sun, J. Y.: Atmospheric aerosol compositions in China: spatial/temporal variability, chemical signature, regional haze distribution and comparisons with global aerosols, Atmos. Chem. Phys., 12, 779-799, https://doi.org/10.5194/acp-12-779-2012, 2012b.
Zhang, X., Chen, Z. M., He, S. Z., Hua, W., Zhao, Y., and Li, J. L.: Peroxyacetic acid in urban and rural atmosphere: concentration, feedback on PAN-NO_x cycle and implication on radical chemistry, Atmos. Chem. Phys., 10, 737-748, https://doi.org/10.5194/acp-10-737-2010, 2010.
Zhang, X., He, S. Z., Chen, Z. M., Zhao, Y., and Hua, W.: Methyl hydroperoxide (CH_3OOH) in urban, suburban and rural atmosphere: ambient concentration, budget, and contribution to the atmospheric oxidizing capacity, Atmos. Chem. Phys., 12, 8951-8962, https://doi.org/10.5194/acp-12-8951-2012, 2012a.
Zhang, Y., Bao, F., Li, M., Chen, C., and Zhao, J.: Nitrate-Enhanced Oxidation of SO_2 on Mineral Dust: A Vital Role of a Proton, Environ. Sci. Technol., 53, 10139-10145, https://doi.org/10.1021/acs.est.9b01921, 2019b.
Zhao, P. S., Dong, F., He, D., Zhao, X. J., Zhang, X. L., Zhang, W. Z., Yao, Q., and Liu, H. Y.: Characteristics of concentrations and chemical compositions for $PM_{2.5}$ in the region of Beijing, Tianjin, and Hebei, China, Atmos. Chem. Phys., 13, 4631-4644, https://doi.org/10.5194/acp-13-4631-2013, 2013.
Zheng, B., Zhang, Q., Zhang, Y., He, K. B., Wang, K., Zheng, G. J., Duan, F. K., Ma, Y. L., and Kimoto, T.: Heterogeneous chemistry: a mechanism missing in current models to explain secondary inorganic aerosol formation during the January 2013 haze episode in North China, Atmos. Chem. Phys., 15, 2031-2049, https://doi.org/10.5194/acp-15-2031-2015, 2015.
Zheng, H., Song, S., Sarwar, G., Gen, M., Wang, S., Ding, D., Chang, X., Zhang, S., Xing, J., Sun, Y., Ji, D., Chan, C. K., Gao, J., and McElroy, M. B.: Contribution of Particulate Nitrate Photolysis to Heterogeneous Sulfate Formation for Winter Haze in China, Environ. Sci. Technol. Lett., 7, 632-638, https://doi.org/10.1021/acs.estlett.0c00368, 2020.
Zhou, L., Wang, W., Gai, Y., and Ge, M.: Knudsen cell and smog chamber study of the heterogeneous uptake of sulfur dioxide on Chinese mineral dust, J. Environ. Sci.-China, 26, 2423-2433, https://doi.org/10.1016/j.jes.2014.04.005, 2014.
Zhu, L., Jacob, D. J., Eastham, S. D., Sulprizio, M. P., Wang, X., Sherwen, T., Evans, M. J., Chen, Q., Alexander, B., Koenig, T. K., Volkamer, R., Huey, L. G., Le Breton, M., Bannan, T. J., and Percival, C. J.: Effect of sea salt aerosol on tropospheric bromine chemistry, Atmos. Chem. Phys., 19, 6497-6507, https://doi.org/10.5194/acp-19-6497-2019, 2019.